Theory and Operation of a Proton-Spin Refrigerator*

K. H. LANGLEY† AND C. D. JEFFRIES‡
Department of Physics, University of California, Berkeley, California
(Received 20 June 1966)

By rotating a crystal of (Yb, Y)$(C_2H_5SO_4)_3\cdot 9H_2O$ (abbreviated as Yb:YES) at 60 rps in a magnetic field of 10 kOe at 1.4°K, nuclear polarizations as large as 19% are observed for the protons in the H_2O and C_2H_5 groups. This comes about because the Yb^{3+} ions have both an anisotropic g factor ($g_{\parallel}=3.35$, $g_{\perp}\approx 0$) and an anisotropic spin-lattice relaxation rate $\propto \cos^2\theta \sin^2\theta$, allowing the Yb^{3+} polarization at $\theta=45°$ to be transferred to the protons by cross relaxation at $\theta=90°$; cyclic repetition of this is a "spin refrigerator," which can, in principle, maintain a nuclear-spin polarization comparable to an electron-spin polarization. The paramagnetic and relaxation properties of Yb:YES are discussed in detail. Proton relaxation is studied and found to agree approximately with theoretical expectations. A general rate-equation theory of spin refrigerators is developed and used to interpret the measurements in Yb:YES. Although the present polarizations are limited by insufficient rotation speed and multiple spin flips, it is apparent that Yb:YES is a favorable substance, and that polarizations of ~50% might be achieved at higher fields and higher speeds; application to polarized targets is suggested.

I. INTRODUCTION

THE method of dynamic nuclear orientation involving microwave pumping of certain forbidden transitions has produced sizeable polarization of the protons in hydrated crystals[1,2]; this method is currently being used in large polarized targets.[3–6] However, the relative complexity has led to consideration of simpler schemes for polarizing nuclei: nuclear-spin refrigerators.[7,8] In one basic type the nuclei are polarized simply by rotating a crystal in a magnetic field at low temperatures. To fix ideas we immediately consider the crystal which is treated in detail in this paper: yttrium ethyl sulfate, $Y(C_2H_5SO_4)_3\cdot 9H_2O$, in which a few percent of diamagnetic Y^{3+} ions have been replaced by paramagnetic ytterbium Yb^{3+}, added to the growing solution; we denote such crystals by Yb:YES. Figure 1 shows the experimental arrangement to keep in mind: the crystal is immersed in liquid helium at $T\sim 1$°K, and is mounted on a rotatable shaft in a magnetic field $\mathbf{H}\sim 10^4$ Oe, so that the angle θ between $\mathbf{H}$ and the crystal c axis may take any value. A fixed vertical rf coil is used to measure the proton nuclear-magnetic-resonance absorption (NMR) which is just proportional to the proton polarization.

In an elementary exposition of the operation of the spin refrigerator, we speak of the Yb^{3+} ions as Yb "spins," meaning that they constitute a two-level electron-spin system, with effective spin $S=\frac{1}{2}$, but with a very anisotropic g factor:

$$g(\theta)=[g_{\parallel}^2\cos^2\theta+g_{\perp}^2\sin^2\theta]^{1/2},$$

where $g_{\parallel}=3.35$, and $g_{\perp}$ is as small as the proton g factor $g_n=0.00304$. The numerous protons in the waters of hydration and in the ethyl groups form a proton-spin system, $I=\frac{1}{2}$, with two energy levels, Fig. 2(c), separated by $g_n\beta H$ for any value of θ, where β is the Bohr magneton. On the other hand the Yb spins energy splitting $g(\theta)\beta H$ varies greatly with θ, and furthermore they have an anisotropic spin-lattice relaxation time

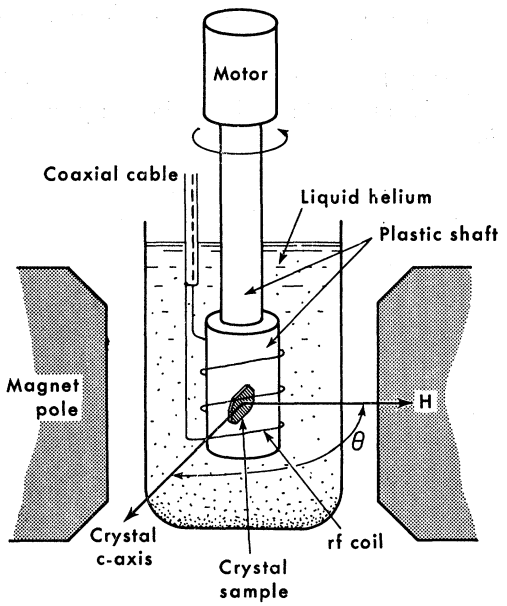

FIG. 1. Experimental arrangement for a spin refrigerator in which a crystal is rotated in a magnetic field.

* Supported in part by the U. S. Atomic Energy Commission and the Office of Naval Research.
† Present address: Department of Physics, University of Massachusetts, Amherst, Massachusetts.
‡ NSF Fellow, 1965–1966, in Division of Applied Physics, Pierce Hall, Harvard University, Cambridge, Massachusetts.
[1] See, e.g., C. D. Jeffries, *Dynamic Nuclear Orientation* (John Wiley & Sons, Inc., New York, 1963).
[2] T. J. Schmugge and C. D. Jeffries, Phys. Rev. **138**, A1785 (1965).
[3] O. Chamberlain, C. D. Jeffries, C. H. Schultz, G. Shapiro, and L. Van Rossum, Phys. Letters **7**, 293 (1963); O. Chamberlain, C. Schultz, and G. Shapiro, in *Proceedings of the 12th Annual International Conference on High Energy Physics, Dubna, 1964* (Atomizdat, Moscow, 1965).
[4] M. Borghini, M. Odehnal, P. Roubeau, C. Ryter, G. Coignet, L. Dick, and L di Lella, in *Proceedings of the 12th Annual International Conference on High Energy Physics, Dubna, 1964* (Atomizdat, Moscow, 1965).
[5] A. Abragam and M. Borghini, *Progress in Low Temperature Physics* (North-Holland Publishing Company, Amsterdam, 1964), Vol. 4.
[6] C. D. Jeffries, Ann. Rev. Nucl. Sci. **14**, 101 (1964).
[7] C. D. Jeffries, Cryogenics **3**, 41 (1963).
[8] A. Abragam, Cryogenics **3**, 42 (1963).

$T_{1e} \propto [\cos^2\theta \sin^2\theta]^{-1}$ which is a minimum at $\theta=45°$, with the typical value 10^{-3} sec. Thus if θ is held at 45° a short time the relative Boltzmann populations shown in Fig. 2(a) are quickly established, where $\Delta = g(45°)\beta H/kT$ and $e^{\Delta} \sim 10$, typically. That is, lattice thermal vibrations induce spin flips preferentially to the lower level, so that the Yb spins quickly become highly polarized parallel to **H**. If we now rotate the crystal to $\theta=90°$ quickly compared to T_{1e} but slowly compared to the Larmor period, i.e., adiabatically in the Ehrenfest sense, the Yb spins will remain polarized along **H**. The levels and populations are as shown in Fig. 2(b); T_{1e} is here very long. A Yb spin now finds itself on speaking terms with a neighbor proton, i.e., through their dipole-dipole coupling they are able to engage in a mutual spin flip which conserves energy, the Yb flipping up, the proton down, as shown by the dotted lines. This process polarizes that proton along **H**. Next the crystal is quickly rotated to 135°, where the Yb spin again gets flipped to the lower state by spin-lattice relaxation; rotation to 180° again polarizes another proton, etc., so that after N_n/N_e cycles all the protons in the crystal become polarized, where N_n/N_e is the relative abundance of protons to Yb spins. More exactly, the proton polarization becomes

$$p_n = \frac{N(m=+\frac{1}{2}) - N(m=-\frac{1}{2})}{N(m=+\frac{1}{2}) + N(m=-\frac{1}{2})} = \frac{e^{\Delta}-1}{e^{\Delta}+1} = \tanh\tfrac{1}{2}\Delta. \quad (1)$$

This exceeds the static thermal equilibrium polarization $p_{n0} = g_n\beta H/2kT$ by $g(45°)/g_n \sim 10^3$; the spin refrigerator is thus potentially as effective as the dynamic microwave method in polarizing nuclei. The protons will of course be depolarized by spin-lattice relaxation, but at a much slower rate than the polarization process. The preliminary operation of a Yb:YES spin refrigerator has been briefly reported earlier.[9]

An alternative, more generalized, description of the refrigerator using the concept of spin temperature[10] is illustrated in Fig. 3, a thermal block diagram of the weakly interacting systems: proton spins, Yb spins, crystal lattice phonons, and helium bath. The protons have a common spin temperature T_n, defined by $p_n \equiv g_n\beta H/2kT_n$; similarly T_e is the Yb spin temperature; and T is the phonon temperature, here assumed to be that of the bath, although this is not always justified, as in the phonon bottleneck case.[11] Thermal switch S_1 schematically represents the Yb spin-lattice relaxation, and is closed at 45°, 135°, ···. Switch S_2 represents the cross relaxation,[12] i.e., the mutual proton-Yb spin flips which occur when $g_n \approx g$; S_2 is closed only at 90°, 270°, ···. The Yb spins are an anisotropic working substance cyclically transfering heat from the protons

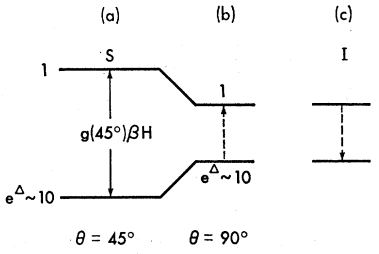

FIG. 2. (a) Energy levels of Yb spins at 45°; (b) energy levels of Yb spins at 90°, showing mutual spin flips with protons as dashed lines; (c) energy levels of protons.

to the bath as θ takes on the successive values 45°, 90°, 135°, ···. At 45°, $T_e \rightarrow T$. Then as $\theta \rightarrow 90°$, S_1 opens and the Yb spins are isentropically cooled[13,14] by virtue of the anisotropy in $g(\theta)$, according to the relation

$$g(45°)/T_e(45°) = g(90°)/T(90°). \quad (2)$$

For Yb:YES we expect $T_e(90°) = T_e(45°)$ $[0.003/3.35 \cos 45°] \approx 10^{-3}$°K. At 90° S_2 closes, putting the cold Yb spins into thermal contact with the proton spins, initially at $T_n = T \approx 1$°K. Conservation of energy requires the calorimetry relation[10] for the common temperature T_c after mixing

$$N_n/T_n + N_e/T_e(90°) = (N_n+N_e)/T_c. \quad (3)$$

For $(N_n/N_e) \sim 10^3$, we find $T_c \approx 0.5$°K, i.e., the proton polarization is increased twofold. After many cycles $T_n \rightarrow T_e(90°)$, leading to the proton polarization of Eq. (1). We note the relation to the earlier spin engine of Bloembergen.[15]

To generalize, the method may be described as a solid-state quantum-mechanical spin refrigerator. One external parameter $\theta = \angle H$, c automatically operates S_1 and S_2 in the proper sequence and at the same time takes the Yb spins through an isentropic cooling cycle. The internal microscopic switches are quantum-mechanical in the sense that they operate by virtue of the dependence of the spin wave functions of Yb^{3+} on the angle θ. Energy is taken from the protons in quanta $g_n\beta H$ and exhausted as phonons of energy $g(45°)\beta H$, which travel with the velocity of sound to the helium bath. The refrigerator can easily operate at 10^3 cps, but only the spins, not the lattice, are cooled. All of these properties clearly distinguish it from the classical magnetic refrigerator, i.e., lattice cooling by adiabatic demagnetization.[16,14] Other nuclei in the crystal besides the protons could be similarly polarized. There are many possible varieties of spin refrigerators: e.g., one could operate S_1 not only by θ but by the magnitude of H, light, pressure, temperature, or electric fields; the electron-spin splitting could be varied by the

[9] K. H. Langley and C. D. Jeffries, Phys. Rev. Letters **13**, 808 (1964).
[10] A. Abragam and W. G. Proctor, Phys. Rev. **109**, 1441 (1958).
[11] P. L. Scott and C. D. Jeffries, Phys. Rev. **127**, 32 (1962).
[12] N. Bloembergen, S. Shapiro, P. S. Pershan, and J. O. Artman, Phys. Rev. **114**, 445 (1959).
[13] G. S. Bogle, A. H. Cooke, and S. Whitley, Proc. Phys. Soc. (London) **A64**, 931 (1951).
[14] T. L. Estle, H. R. Hart, Jr., and J. C. Wheatley, Phys. Rev. **112**, 1576 (1958).
[15] N. Bloembergen, in *Proceedings of the VII International Conference on Low Temperature Physics* (University of Toronto Press, Toronto, Canada, 1961), p. 36.
[16] W. F. Giauque and D. P. MacDougall, Phys. Rev. **43**, 768 (1933).

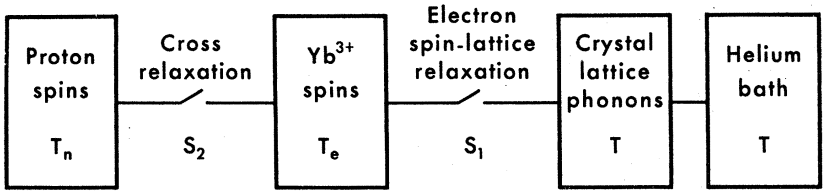

FIG. 3. Thermal block diagram for a spin refrigerator.

magnitude of H in third-order Zeeman splitting, or by level crossing.

Instead of quickly switching θ to the discrete values 45°, 90°, ···, as implied by our elementary exposition, one may continuously rotate the crystal by a motor; the expected proton polarization is still roughly given by Eq. (1). We have observed proton polarizations as high as ~19% in Yb:YES by rotation at $f_r=60$ rps, which is the upper practical speed limit for our apparatus, due to friction and vibration. The limitation in polarization is partly due to insufficient speed, and McColl[17] has recently obtained 35% proton polarization in the same crystals by effectively rotating the net field rather than the crystal at $f_r\sim10^3$ cps, by a superposition of dc and pulsed fields. It is clear that Yb:YES is a favorable substance for a spin refrigerator and so we present in Sec. III the details of the paramagnetic and relaxation properties, including a discussion of why $g(\theta)$ and $T_{1e}(\theta)$ are so anisotropic. In Sec. IV we compare theory and measurements of the proton relaxation rate. Finally in Sec. V, we consider a coupled I, S system and the general dynamical behavior of spin refrigerators; this is compared in Sec. VI to measurements for continuous rotation of Yb:YES.

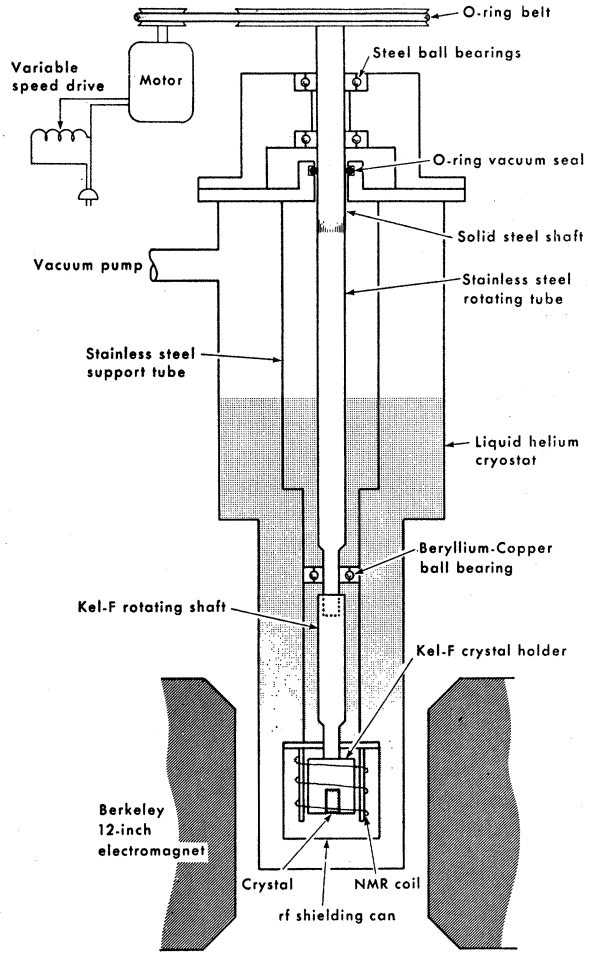

FIG. 4. Apparatus for rotating crystals in a magnetic field.

[17] J. R. McColl and C. D. Jeffries, Phys. Rev. Letters **16**, 316 (1966).

Actually the first substance we considered was 1% Ce in $La_2Mg_3(NO_3)_{12}\cdot24H_2O$ (hereafter abbreviated Ce:LaMN), which also has both anisotropic relaxation rate and anisotropic g factor ($g_\perp=1.83$, $g_{11}\sim0$). Rotation in $H\approx20$ kOe, at speeds up to $f_r\sim60$ rps, and $T\approx1.3$°K did not yield any significant proton enhancements.[18] Paramagnetic resonance measurements at 80 Mc/sec were then performed, yielding $g_{11}=0.023\pm0.0002$, which is 7× larger than g_n, so that cross relaxation did not occur. Subsequent rotation experiments by Robinson[19] gave polarizations of ~0.1% in low fields, where there is some overlap between the proton resonance line and the tail of the Ce^{3+} line. Further experiments[20,21] on Ce:LaMN have not yielded proton polarizations greater than a few percent. Besides being much more anisotropic, Yb:YES has the advantage that the g factor is small in a plane rather than along a single axis, thus simplifying the crystal orientation problem considerably. Rotation of $Cr:Al_2O_3$ has produced ~1% polarization of Al^{27} nuclei.[22]

II. APPARATUS AND CRYSTALS

Figure 4 depicts some of the details of the apparatus. A Yb:YES single crystal is mounted in a Kel-F plastic (Minnesota Mining & Manufacturing Company) holder at the end of a motor driven shaft installed in a metal helium Dewar; the liquid-N_2 shield is not shown. The

[18] We are indebted to Dr. T. J. Schmugge for his helpful collaboration in these early experiments, described in 1 September 1962 and 1 December 1962 Status Reports, Office of Naval Research Contract Nonr 222(61), University of California, Berkeley (unpublished).

[19] F. N. H. Robinson, Phys. Letters **4**, 180 (1963).

[20] J. Combrisson, J. Ezratty, and A. Abragam, Compt. Rend. **257**, 3860 (1963).

[21] V. I. Lushchikov, B. S. Neganov, L. B. Parfenov, and Yu. V. Taran, Zh. Eksperim. i Teor. Fiz. **49**, 406 (1965) [English transl.: Soviet Phys.—JETP **22**, 285 (1966)].

[22] W. G. Clark, G. Feher, and M. Weger, Bull. Am. Phys. Soc. **8**, 463 (1963).

TABLE I. Yb:$Y(C_2H_5SO_4)_3 \cdot 9H_2O$ crystals used in the experiments. Brackets indicate crystals grown simultaneously in the same solution.

Crystal number	Concentration of Yb	Chemical Y	Source Yb
[1	10% natural	a	c
2]	10% natural	a	c
3	0.5% natural	a	c
[4	2% natural	a	c
5]	2% natural	a	c
[6	2% natural	a	c
7]	2% natural	a	c
8	0.2% enriched	b	d
[9	2% enriched	b	d
10]	2% enriched	b	d
11	5% enriched	b	d

Chemical	Source
a. Y_2O_3	Research Chemicals Division, Nuclear Corporation of America. $Y \sim 99.9999\%$.
b. $Y_2(SO_4)_3 \cdot 8H_2O$	Lindsay Chemical Company, Code 1148; $Y \sim 99.9999\%$ principal impurities Gd, Tb, Dy.
c. $Yb_2(SO_4)_3 \cdot 8H_2O$	Lindsay Chemical Company, Code 1242; Yb~99.9% principal impurities Er, Tm, Lu.
d. Yb_2O_3	Oak Ridge National Laboratory, series *KJ*, sample 1245(*A*); enriched to 97.1% Yb^{172} isotope.
H_2SO_4[a]	Mallinckrodt analytical reagent, code 2876; $Fe \approx 0.00002\%$.
$Ba(C_2H_5SO_4)_2 \cdot 2H_2O$[a]	City Chemical Corporation, electronic grade; Ba~99.999%, Fe<0.0006%, Cr<0.0018%

[a] Used in synthesizing the ethyl-sulfate from the sulfate.

beryllium-copper ball bearings (New Hampshire No. NR4K25) were carefully degreased to prevent freezing; the lower bearing is simply a close-fitting hole in a brass plate through which the shaft passes. Kel-F was used for the shaft, crystal holder, and NMR coil because it contains no protons, is accurately machineable, and is nonconducting, which eliminates eddy-current heating. Although rotation speeds of at least 90 rps could be obtained, vibration and heating limited the useful upper limit to $f_r \sim 60$ rps, corresponding to a heat input of ~300 mW. Helium temperatures down to $T \approx 1.4$°K could be maintained with an 80-ft³/min mechanical pump. The Dewar was installed in the $1\frac{5}{8}$-in. gap of a Berkeley 12-in. electromagnet, which produced fields up to 22 kOe.

The proton NMR absorption signal was observed with the Q-meter circuit previously described.[2] Magnetic-field modulation at 270 cps, and a lock-in detector were used to record the derivative signal on a paper tape, allowing for a monitoring of the proton polarization as it built up upon rotation, or decayed through relaxation at rest.

Two types of crystals were used: (1) Yb^{172}:YES grown from Yb enriched to 97.1% Yb^{172} which has no nuclear spin, so that the electron-spin system is closely

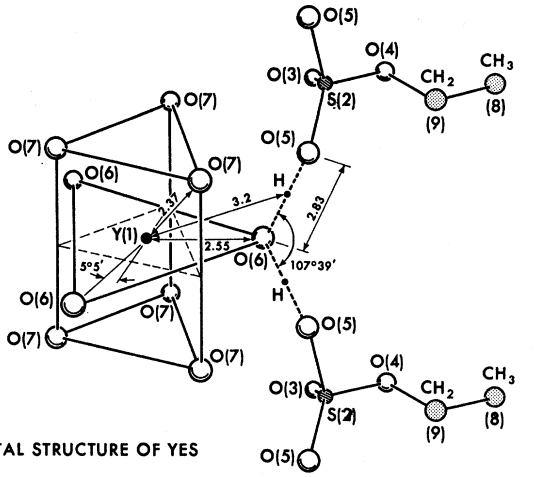

FIG. 5. Crystal structure of YES, constructed from the data of Ref. 26; distances are in Å. The positions of the H atoms are somewhat uncertain.

represented by the two-level scheme assumed in Sec. I. (2) Yb:YES grown from Yb of natural isotopic abundance, containing 14% Yb^{171} ($I=\frac{1}{2}$) and 16% Yb^{173} ($I=\frac{5}{2}$), which give hyperfine lines superimposed on the two Zeeman levels, which may complicate the cross relaxation at $\theta \approx 90°$. The crystals used are listed in Table I, along with the sources of chemicals and the impurities. Other studies[2,11,23] indicate that high purity is required to avoid extraneous relaxation from traces of magnetic impurities such as Fe^{2+}, Ce^{3+}, Pr^{3+}, which have very short relaxation times. For this reason we have preferred yttrium rather than lanthanum ethyl sulfate (LaES) because it is available in higher purity. Erath's procedure[24] was used to synthesize the ethyl sulfates. Crystals were grown from saturated aqueous solution in a desiccator at 0°C. The % Yb in Table I is that of the fresh growing solution. The crystals were somewhat irregular, typically 2 mm thick by 6 mm in diameter, weighing ~100 mg. The c-axis direction was confirmed by x-ray back-reflection Laué photographs, and the crystals mounted in the holder, Fig. 4, with the c axis horizontal to within a few degrees.

III. PARAMAGNETIC RESONANCE AND RELAXATION IN Yb:YES

A. Paramagnetic Properties

Crystal structure. The original ethyl sulfate structure determinations[25] have been refined for YES by Fitzwater and Rundle,[26] with the results shown in Fig. 5. Y atoms are at the center of a triangle of $O(6)$ atoms, with two more triangles $O(7)$ above and below. All the heavy

[23] G. H. Larson and C. D. Jeffries, Phys. Rev. **141**, 461 (1966); **145**, 311 (1966).
[24] E. H. Erath, J. Chem. Phys. **34**, 1985 (1961).
[25] J. A. A. Ketelaar, Physica **4**, 619 (1937).
[26] D. R. Fitzwater and R. E. Rundle, Z. Krist. **112**, 362 (1959).

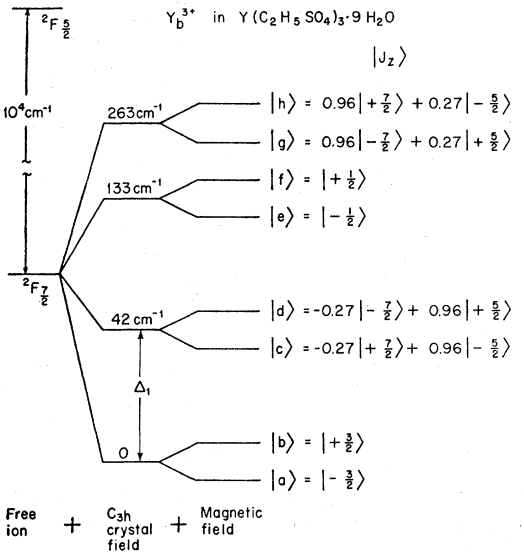

FIG. 6. Levels of Yb^{3+} in the ethyl-sulfate crystal.

atoms and probably even the hydrogens are in the $P6_3/m$ space group; the nearest Y-H distance is ~ 3.2 Å. Extensive paramagnetic resonance and optical spectroscopy data indicate that a majority of rare-earth ions substitute for Y in YES, and that there is only one magnetic site, of C_{3h} (i.e., $\bar{6}$) symmetry similar to LaES, which is isostructural with YES. However, paramagnetic-resonance studies[27,28] in Dy:LaES seem to indicate that besides this site there may be six other sites of lower symmetry due to a slight distortion. We assume that these spurious sites occur only infrequently and neglect them in the following. We also assume that the discussion for concentrated YbES also applies to dilute Yb:YES, with exceptions noted.

Energy levels. The Yb^{3+} free ion $4f^{13}$ has a $^2F_{7/2}$ ground state and Landé g factor $\Lambda=8/7$; the spin-orbit interaction $\mathcal{H}_{so}$ places the next multiplet $^2F_{5/2}$ higher by 10 200 cm^{-1}. Figure 6 shows the further splitting of the ground multiplet by the ethyl sulfate crystal-field Hamiltonian $\mathcal{H}_c$; only the first splitting $\Delta_1=42$ cm^{-1} has been measured optically.[29] The Zeeman interaction $\mathcal{H}_Z=\Lambda\beta\mathbf{H}\cdot\mathbf{J}$ lifts the degeneracy of the Kramers doublets. Only the lowest doublet $|a\rangle$, $|b\rangle$ is significantly populated at helium temperatures, and forms the effective $S=\frac{1}{2}$ electron-spin system introduced in Sec. I. In the standard crystal field theory for the ethyl sulfates[30] the Hamiltonian is taken to be

$$\mathcal{H}_c=A_2^0\langle r^2\rangle\alpha O_2^6+A_4^0\langle r^4\rangle\beta O_4^0+A_6^0\langle r^6\rangle\gamma O_6^0 + A_6^6\langle r^6\rangle\gamma O_6^6, \quad (4)$$

where $A_n^m\langle r^n\rangle$ are crystal field parameters; α, β, and γ are operator equivalent factors[31]; and O_n^m are certain operators[32] in J_z, $J_\pm$. Since $\mathcal{H}_{so}\gg\mathcal{H}_c$, J is a good quantum number; one uses $|J=\frac{7}{2}, J_z\rangle$ as basis functions for the $^2F_{7/2}$ doublets, where z is the crystal c axis. Although the $A_n^m\langle r^n\rangle$ could in principle be determined by spectroscopy, there are not yet enough data and we must resort to approximation.

By an empirical extrapolation procedure[30,33] using the $A_n^m\langle r^n\rangle$ parameters for the concentrated ethyl sulfates,[34] we obtain for YbES the values $A_2^0\langle r^2\rangle=140$, $A_6^0\langle r^6\rangle=-29$, and $A_6^6\langle r^6\rangle=410$ cm^{-1}. As the extrapolation of $A_4^0\langle r^4\rangle$ is somewhat ambiguous we determined it by diagonalizing $\mathcal{H}_c$ in the $J=\frac{7}{2}$ manifold, subject to the condition $\Delta_1=42$ cm^{-1}; this yields $A_4^0\langle r^4\rangle=-68$ cm^{-1} and the wave functions $|J_z\rangle$ shown in Fig. 6. For the lowest doublet the predicted g factors are $g_{11}=2\Lambda\langle a|J_z|a\rangle=3.43$, and $g_\perp=\Lambda\langle a|J_+ + J_-|b\rangle=0$; low-temperature susceptibility measurements[35,36] in YbES give $g_{11}=3.40\pm0.07$ and $g_\perp<0.05$. This confirms the prediction[30] that $|\pm\frac{3}{2}\rangle$ is the lowest doublet since $g_\perp\gtrsim 1$ for the others. Although the fact that $|\pm\frac{3}{2}\rangle$ is the lowest doublet depends on the relative magnitude of the crystal field parameters, the fact that $g_\perp$ is zero is a consequence of the *symmetry*: For C_{3h} only states differing by $\Delta J_z=\pm 6$ are admixed and since $J_z\leqq J=\frac{7}{2}$, this does not allow $|\pm\frac{3}{2}\rangle$ to be admixed to any other states; $|\pm\frac{3}{2}\rangle$ has no matrix elements for $J_\pm$, hence $g_\perp=0$.

Paramagnetic resonance. Since the microwave transition probability between $|a\rangle$ and $|b\rangle$ is proportional to $g_\perp^2$, one would not expect to observe paramagnetic resonance, and none was reported until Schmugge[27] using high microwave fields observed a weak resonance at $\theta=0$ in YbES and in Yb:LaES, corresponding to $g_{11}=3.35$. It is not yet clear whether these arise from Yb ions in purely C_{3h} sites or from distorted sites of lower symmetry, for which $g_\perp>0$.

Third-order corrections. Even for C_{3h} sites the value of $g_\perp$ must not entirely vanish, because the above calculation is really only zero order: it uses crystal field eigenfunctions and does not take into account admixing due to the Zeeman interaction. We now take at $\theta=90°$, $\mathcal{H}_Z=\Lambda\beta H_x(J_+ + J_-)/2$ and the functions $|a_\perp\rangle=[|\frac{3}{2}\rangle - |-\frac{3}{2}\rangle]/\sqrt{2}$, $|b_\perp\rangle=[|\frac{3}{2}\rangle + |-\frac{3}{2}\rangle]/\sqrt{2}$, etc. which are diagonal in $\mathcal{H}_Z$. Using standard perturbation theory[37] to third order we find the energy splitting $E_3=|E_b-E_a|$

[27] T. J. Schmugge (private communication).
[28] Joel A. Dweck, thesis, Brown University, Providence, Rhode Island, 1965 (unpublished).
[29] E. Y. Wong, J. Chem. Phys. **39**, 2781 (1963).
[30] R. J. Elliott and K. W. H. Stevens, Proc. Roy. Soc. (London) **A215**, 437 (1952); **A218**, 553 (1953); **A219**, 387 (1953).
[31] K. W. H. Stevens, Proc. Phys. Soc. (London) **A65**, 209 (1952).
[32] R. Orbach, Proc. Roy. Soc. (London) **A264**, 458 (1961).
[33] M. J. D. Powell and R. Orbach, Proc. Phys. Soc. (London) **78**, 753 (1961).
[34] S. Hüfner, Z. Physik **169**, 417 (1962).
[35] A. H. Cooke, F. R. McKim, H. Meyer, and W. P. Wolf, Phil. Mag. **2**, 928 (1957).
[36] J. Van den Broek and L. C. Van der Marel, Physica **29**, 948 (1963); **30** 565 (1964).
[37] E. U. Condon and G. H. Shortley, *The Theory of Atomic Spectra* (Cambridge University Press, Cambridge, England, 1963).

$\equiv 2qH^3$ Mc/sec, where H is in Oe and

$$q=\left(\frac{\Lambda\beta}{2}\right)^3\sum_{i,j}\frac{\langle b_1|J_+ + J_-|i\rangle\langle i|J_+ + J_-|j\rangle\langle j|J_+ + J_-|b_1\rangle}{\Delta_i\Delta_j}$$
$$\approx 2.25\times10^{-12}, \quad (5)$$

where $|i\rangle$ and $|j\rangle$ are one of the excited states $|c_1\rangle$, $|f_1\rangle$, and $|h_1\rangle$. We find $E_3\approx g_n\beta H$ at $H\approx 30$ kOe, showing that the third-order Zeeman splitting is extremely small in YbES. In DyES, for which $g_{11}=11$, $g_1=0$, the third-order splitting is larger by 10^3. In preliminary spin refrigerator experiments we have not observed any proton polarization in DyES in $\sim$10 kOe, possibly bebecause the third-order splitting is large enough to prevent cross relaxation to the protons.

At small angles $\varphi=90°-\theta$, the total Yb^{3+} Zeeman splitting is $E=(E_3^2+E_1^2)^{1/2}$ due to both the third-order and first-order term $E_1\approx g_{11}\beta H\varphi$. In 10 kOe, the proton splitting equals the Yb^{3+} splitting at $\varphi=0.05°$, the first-order term strongly dominating. As discussed in Sec. IV the observed angular halfwidth of the Yb-proton cross-relaxation peak is $\varphi\approx 0.3°$, probably due to the Yb^{3+} linewidth.

B. Spin-Lattice Relaxation

A quantitative theory of the spin refrigerator requires detailed knowledge of the processes whereby a Yb^{3+} ion in spin state $|b\rangle$ goes to $|a\rangle$. More specifically we wish to know the characteristic relaxation time T_{1e} with which the Yb polarization $p_e=[N(a)-N(b)]/[N(a)+N(b)]$ goes to its termal equilibrium value $p_{e0}=\tanh(g_{11}\beta H\cos\theta/2kT)$. The standard theory[38] of paramagnetic relaxation due to thermal modulation of the crystalline electric fields has been recast in a phenomenological form appropriate for rare-earth ions by Orbach.[32] Extensive measurements[11,23,36,39] on rare-earth ethyl sulfates and double nitrates are in moderate agreement with theoretical estimates. For Kramers ions such as Yb^{3+} the relaxation rate of the lowest doublet may usually be expressed as

$$T_{1e}^{-1}=A''T+Be^{-\Delta/kT}+CT^9 \text{ sec}^{-1}, \quad (6)$$

where the first term, the direct process T_{1d}^{-1}, arises from a spin flip from $|b\rangle$ to $|a\rangle$ and the simultaneous creation of a phonon of energy $h\nu=g\beta H$. The second term, the Orbach process T_{1o}^{-1}, arises from a spin flip from $|b\rangle$ to a higher state $|d\rangle$ at Δ, and then a flip down to $|a\rangle$, accompanied by phonon absorption at Δ and creation at $\Delta+h\nu$. The third term, the Raman process T_{1R}^{-1}, is a higher order process through an excited state. Neither B nor C depend significantly on H or θ, whereas A'' is strongly dependent on both. At $T\leqq 1.5$°K and $H\geqq 2$ kOe, the conditions for our spin refrigerator experiments, the direct process strongly dominates except near $\theta=0°$ and 90°.

[38] J. H. Van Vleck, Phys. Rev. **57**, 426 (1940).

[39] J. M. Baker and N. C. Ford, Jr., Phys. Rev. **136**, A1692 (1964).

TABLE II. Spin-lattice relaxation rates for YbES.

	A	B	C
Hand calculation	1.2×10^{-12}	3.5×10^{11}	1.73×10^{-2}
Computer calculation	1.78×10^{-12}	3.3×10^{11}	1.67×10^{-2}
Measurements		7×10^{11}	1.55×10^{-2}

Anisotropy of the direct process. Since the anisotropy and field dependence of the direct process are of central importance to the operation of spin refrigerators, we indicate how the dependence $A''(\theta,H)$ arises for YbES. Now $T_{1e}^{-1}=w_{b\to a}+w_{a\to b}$, and from time-dependent perturbation theory

$$T_{1d}^{-1}\approx 2\pi\hbar^{-1}\rho(\nu)[|\langle a|\mathcal{H}'|b\rangle|^2+|\langle b|\mathcal{H}'|a\rangle|^2], \quad (7)$$

where $\rho(\nu)$ is the density of states and is just proportional to the number of lattice oscillators per unit frequency, i.e., to ν^2; and $\mathcal{H}'$ is the perturbation due to the thermal modulation of the crystal field and is of order $\mathcal{H}_c$, Eq. (4), multiplied by the thermal strain ϵ. In Eq. (7), the bracketed term will yield a factor $\nu\coth(h\nu/2kT)$ from the strain and a factor $|\langle a|O_n^m|b\rangle|^2$ which vanishes by Kramers' theorem unless $|a\rangle$ and $|b\rangle$ are admixed by the Zeeman perturbation with higher doublets $|i\rangle$ by an amount of order $\langle a|\Lambda\beta H(\cos\theta J_z+\sin\theta J_x)|i\rangle/\Delta$. From Fig. 6 it is evident that only J_x will admix $|a\rangle$ and $|b\rangle$ with other doublets. The over-all result is

$$T_{1d}^{-1}\propto\nu^3\coth(h\nu/2kT)H^2\sin^2\theta. \quad (8a)$$

Using $h\nu\approx g_{11}\beta H\cos\theta$ this becomes

$$T_{1d}^{-1}=A'H^5\sin^2\theta\cos^3\theta\coth(g_{11}\beta H\cos\theta/2kT). \quad (8b)$$

For $g_{11}\beta H\cos\theta\ll 2kT$ this takes the more familiar form

$$T_{1d}^{-1}=AH^4T\sin^2\theta\cos^2\theta. \quad (9)$$

To actually evaluate the constants A in Eq. (9) and B and C in Eq. (6) we have used a previous procedure[11,23] in estimating the magnitude of the dynamic crystal-field parameters from the states parameters. The over-all results of our hand calculations are given in Table II along with a similar calculation performed by Larson[40] using a computer, and the experimental results for YbES of Van den Broek and Van der Marel[36] using the low-frequency susceptibility method. They actually find $T_{1o}^{-1}=5.1\times10^{11}\exp(-59/T)$ but since we use the optically measured value $\Delta=60$°K we have adjusted B to 7×10^{11} which gives a good fit to the data in the significant region near 3°K. The value $A=1.2\times10^{-12}$ in Eq. (9) leads to $A'=1.38\times10^{-16}$ in the more exact expression Eq. (8b). Figure 7 compares the measured and hand-calculated rates for the Orbach and Raman processes; the agreement is acceptable. This figure also

[40] G. H. Larson (private communication); the procedure used in making the calculations is described in detail in Ref. 23.

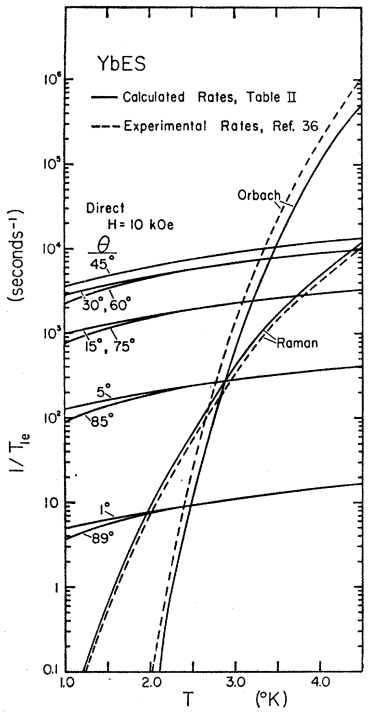

FIG. 7. Theoretical and measured relaxation rates for the lowest Kramers doublet in YbES.

shows the hand-calculated direct rate at $H=10$ kOe for various angles. Although there are some measurements[36] in YbES at low temperatures showing $T_{1e}^{-1}\propto T$ we do not feel that this is the true Van Vleck–Kronig direct process which we have been considering, but rather a Waller[41] process arising from dipolar interactions between Yb^{3+} neighbors, which should be negligible in dilute Yb:YES. As we shall see, there is evidence from the proton relaxation in Yb:YES that the direct process is weaker and the Raman process stronger than indicated by Fig. 7.

Higher order corrections at $\theta=90°$. Just as the zero order calculation yielding $g_\perp=0$ was corrected, so Eq. (8a) must be corrected in higher order at 90° by replacing $h\nu=g_{\parallel}\beta H\cos\theta$ by $h\nu=2qH^3$ from Eq. (5), yielding

$$T_{1d}^{-1})_\perp\approx 1.1\times10^{-36}H^8T\ \text{sec}^{-1}, \qquad (10)$$

where H is in Oe. At $T\sim1$°K, $H\sim10^4$ Oe, this is 10^{-4} sec^{-1}, and is thus completely negligible compared to T_{1R}^{-1} in Fig. 7.

Hyperfine effects. We have implicitly assumed Yb^{172} until now and have neglected any additional relaxation effects for Yb^{171} and Yb^{173} in the direct process arising from admixtures of the Kramers doublets by the $A\mathbf{I}\cdot\mathbf{S}$ interaction.[39] For Yb^{173} we estimate this effect, using a previous notation,[23] to be

$$T_{1\gamma}^{-1}(M=\tfrac{1}{2})=5.3\times10^{-7}H^2T\cos^2\theta\ \text{sec}^{-1}, \qquad (11a)$$

$$T_{1\beta}^{-1}(M=\tfrac{1}{2})=1.7\times10^{-8}H^2T\cos^2\theta[(1-0.6\cos^2\theta)/(1-0.9\cos^2\theta)]\ \text{sec}^{-1}. \qquad (11b)$$

[41] I. Waller, Z. Physik **79**, 370 (1932).

The over-all result is that the relaxation rate is not much affected by hfs effects except near $\theta=0°$, where it may be increased by a factor 5, typically. In Sec. V we shall see that only the relaxation rate between 45° and 90° appreciably affects the proton polarization.

IV. PROTON RELAXATION IN Yb:YES

For 2% Yb:YES the ratio of protons to Yb spins is $N_n/N_e=1650$. In contrast to Yb^{3+} these numerous protons have no electric interaction with the lattice, the Waller process is utterly negligible, and the protons relax only through their coupling with Yb spins. We neglect other, undesirable, paramagnetic impurities. This is a complicated problem which can only be solved approximately. We utilize two different models: the first, appropriate at $\theta\neq90°$ where the Yb spins have an appreciably larger g factor and proton relaxation is predominantly through forbidden I_+S_- transitions in the coupled proton-Yb system; and the second model, appropriate at $\theta\approx90°$, where relaxation is through energy conserving I_+S_- cross relaxation flips.

A. $\theta\neq90°$

We use the shell-of-influence model but with modifications[42] to take into account diffusion of proton polarization.[43] Imagine that all the protons **I** can be grouped into shells $r_1<r<r_2$ about a typical Yb spin **S**, in the sense that **S** is the source of the proton relaxation and, in the spin refrigerator, is also the source of polarization. A single shell, Fig. 8, is representative of the entire crystal. Radius $r_1=3.2$ Å is the minimum I-S spacing; $r_2\approx(4\pi N_e/3)^{-1/3}$ where N_e is the number of Yb spins per cm^3; for 2% Yb, $r_2\approx19$ Å; $r_1'\leqq7$ Å is the radius within which protons are excluded from the NMR

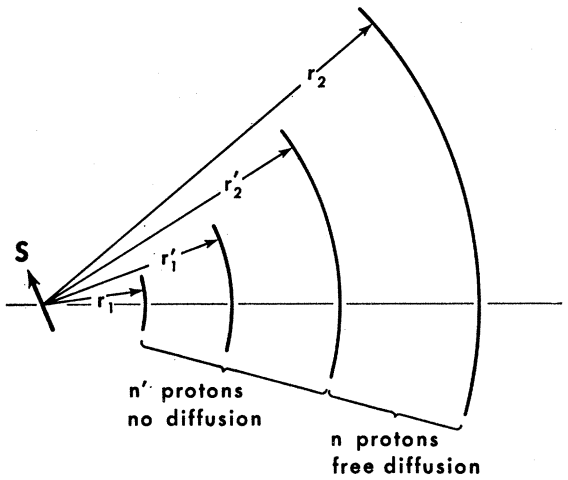

FIG. 8. Shell-of-influence model for proton spins about a Yb spin S.

[42] C. D. Jeffries, Proc. Phys. Soc. (London) **88**, 257 (1966).
[43] N. Bloembergen, Physica **15**, 386 (1949); J. Hatton and B. V. Rollin, Proc. Roy. Soc. (London) **A199**, 222 (1949).

signal by the local field of **S**; $r_2' \leqq 10$ Å is the diffusion barrier[44,45] within which mutual proton flips are inhibited by the local field. There are n "distant" protons spin I between r_2' and r_2 which come into internal equilibrium by diffusion in the short time $t_d \sim 10^{-2}$ sec, typically. There are n' "near" proton spins I' between r_1 and r_2' which interact directly with **S** and have an effective average relaxation rate $(T_{1n}')^{-1}$ to the helium bath through **S**. Figure 9 shows a thermal block diagram, including the coupling of the I and I' systems by a phenomenological cross relaxation rate $(T_{12}')^{-1}$. The rate equations [cf. Eqs. (31)] for the proton polarizations of the coupled systems are

$$\dot{p}_n = -[(p_n - p_n')/T_{12}'](n'/n), \tag{12a}$$

$$\dot{p}_n' = -(p_n' - p_n)/T_{12}' - (p_n' - p_{n0}')/T_{1n}'. \tag{12b}$$

For the reasonable conditions $n' \ll n$ and $T_{12}' \ll T_{1n}'$, the time constants are given by

$$1/T_{1n} \approx (n'/n)(1/T_{1n}') \approx (r_2'/r_2)^3(1/T_{1n}'), \tag{13a}$$

$$1/\tau_f \approx 1/T_{12}'. \tag{13b}$$

The first is to be associated with the abundant distant protons and is expected to be observed. The second is much shorter and is associated with the less-abundant near protons and may be difficult to observe.

Now $(T_{1n}')^{-1}$ can be calculated as previously,[2] but with the additional complication that the g factor is anisotropic: Take **S** at the origin of crystal coordinates (xyz) with the crystal c axis along z, **I** at (r,Θ,Φ), and **H** in the xz plane with $\theta = \angle c, H$. The $I_\pm S_z$ terms of the dipolar interaction admix the zero order states so the the effective Yb spin-lattice relaxation operator $\mathcal{H}'(t) \propto S_+(t)$ can induce both forbidden transitions $w_3(\Delta M_s = 1,\ \Delta m_I = \pm 1)$ and allowed transitions $w_1(\Delta M_s = 1,\ \Delta m_I = 0)$ in the ratio

$$\frac{w_3}{w_1} = \frac{1}{4}\left(\frac{g_{11}\beta}{r^3 H}\right)^2 \{\sin^2\theta(1-3\cos^2\Theta)^2 + \tfrac{9}{2}(1+\cos^2\theta) \times \sin^2\Theta\cos^2\Theta + 6\sin\theta\cos\theta\sin\Theta\cos\Theta(1-3\cos^2\Theta) \times \cos\Phi - \tfrac{9}{2}\sin^2\theta\sin^2\Theta\cos^2\Theta\cos 2\Phi\}. \tag{14}$$

If the near protons are assumed to be isotropically distributed then the spatial average over Θ and Φ and the average value $\langle r^{-6}\rangle = r_1^{-3}(r_2')^{-3}$ may be used to obtain

$$\frac{1}{T_{1n}'} = \frac{1}{20}\left(\frac{g_{11}\beta}{H}\right)^2 \frac{(7-\cos^2\theta)}{r_1^3(r_2')^3} \times \frac{\operatorname{sech}^2\chi}{T_{1e}}, \tag{15}$$

$$\chi \equiv g_{11}\beta H\cos\theta/2kT. \tag{16}$$

We take $7 - \cos^2\theta \approx 6$ and from Eq. (13a) find that

$$\frac{1}{T_{1n}} \approx \frac{3}{10}\left(\frac{g_{11}\beta}{H}\right)^2 \frac{1}{r_1^3 r_2^3} \frac{\operatorname{sech}^2\chi}{T_{1e}}. \tag{17}$$

[44] W. E. Blumberg, Phys. Rev. **119**, 79 (1960).
[45] G. R. Khutsishvili, Zh. Eksperim. i Teor. Fiz. **42**, 1311 (1962) [English transl.: Soviet Phys.—JETP **15**, 909 (1962)].

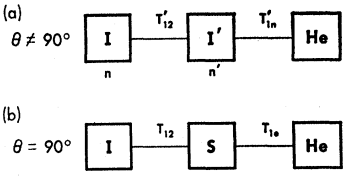

FIG. 9. Thermal block diagrams (a) for $\theta \neq 90°$; (b) for $\theta = 90°$.

This result is not critically dependent on the diffusion barrier r_2', and is essentially the same as Eq. (14) of Ref. 2. We conclude that consideration of diffusion leads to a unique relaxation rate of the same magnitude as the average rate in the shell-of-influence model. Although diffusion is important in establishing equilibrium among the distant nuclei, it is so rapid that it does not enter explicitly into the observed rate, which is determined rather by the direct interaction of the nearest protons with the Yb^{3+} ion.

If the assumption of isotopic distribution of **I** leading to Eq. (15) and Eq. (17) were not made, a more exact expression could be obtained by substituting for $(7-\cos^2\theta)/20r_1^3(r_2')^3$ in Eq. (15) the expression obtained by summing Eq. (14) directly over the n' near protons:

$$\frac{1}{4n'}\sum_i r_i^{-6}\{\sin^2\theta(1-3\cos^2\Theta_i)^2 + \tfrac{9}{2}(1+\cos^2\theta)\sin^2\Theta_i \times \cos^2\Theta_i + 6\sin\theta\cos\theta\sin\Theta_i\cos\Theta_i(1-3\cos^2\Theta_i) \times \cos\Phi_i - \tfrac{9}{2}\sin^2\theta\sin^2\Theta_i\cos^2\Theta_i\cos 2\Phi_i\}. \tag{18}$$

This could be computed if the proton positions were known well enough.

B. $\theta \approx 90°$

As $\theta \to 90°$, the Yb^{3+} splitting approaches the proton splitting, the zero order wave functions become completely admixed and the above model breaks down. We now represent the system by the thermal block diagram of Fig. 9(b): the protons are coupled together by rapid polarization diffusion, and are coupled by cross relaxation at the rate T_{12}^{-1} [defined in Eq. (30)] to the spins **S**, which now only weakly relax at the rate $T_{1e}^{-1}(90°)$ to the lattice, assumed to be closely coupled to the helium bath. The levels are shown in Fig. 13 and the rate equations lead to the two time constants [cf. Eqs. (33)]

$$1/\tau_s \approx (N_e/N_n)[1/(T_{1e}+T_{12})], \tag{19a}$$

$$1/\tau_f \approx 1/T_{12} + 1/T_{1e}, \tag{19b}$$

assuming $N_e \ll N_n$. Although the Yb^{3+} spins and protons display both time constants, the principal change in the Yb^{3+} occurs in τ_f, while the principal change in the proton polarization occurs in time τ_s.

C. Measurements and Interpretation

To summarize the above prediction at $\theta \neq 90°$, the proton relaxation rate is given by Eq. (17), which

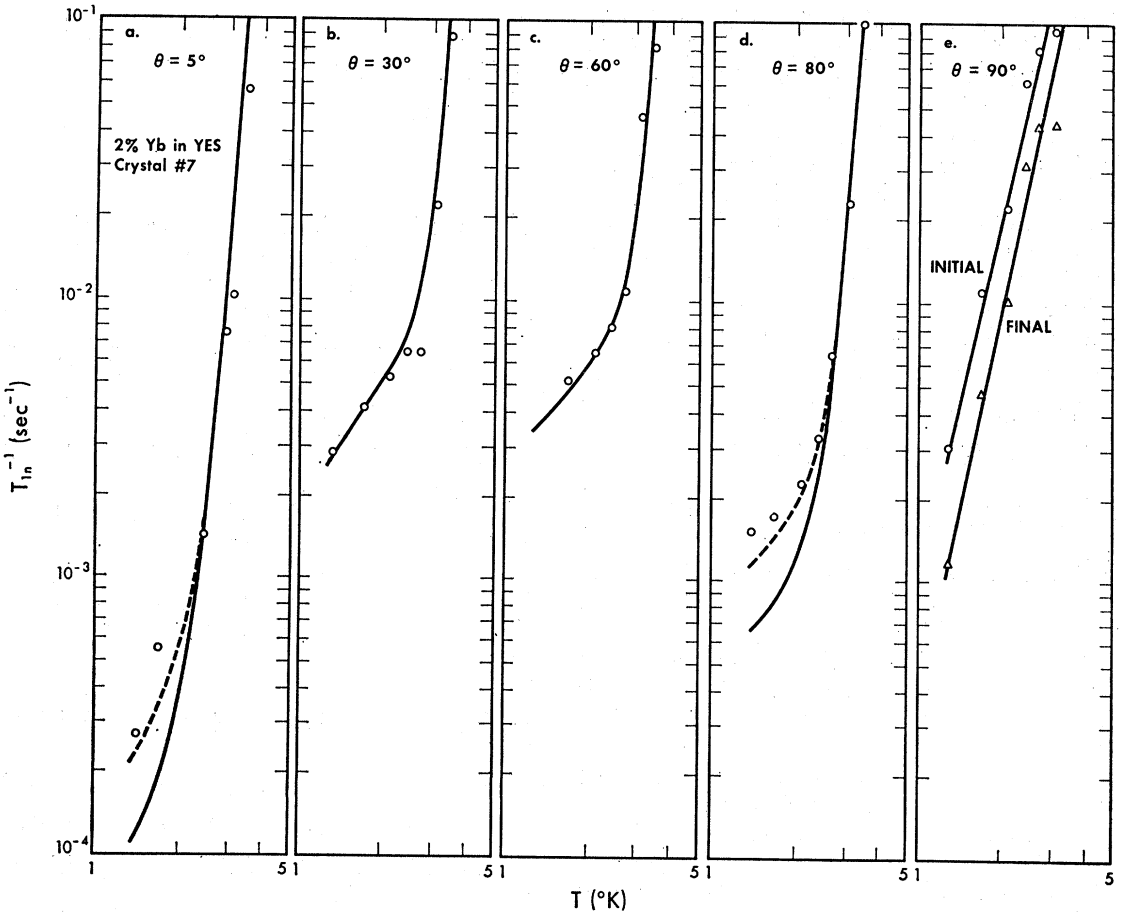

FIG. 10. Measured proton relaxation rate T_{1n}^{-1} in 2% Yb:YES versus temperature T, at $H=10$ kOe for various orientations. The solid lines in (a), (b), (c), and (d) are Eq. (21).

becomes

$$T_{1n}^{-1}=13.5\times10^{2}H^{-2}[1.38\times10^{-16}H^{5}\sin^{2}\theta\cos^{3}\theta\coth\chi+7\times10^{11}\exp(-60/T)+1.5\times10^{-2}T^{9}]\times\operatorname{sech}^{2}\chi\ \sec^{-1},\quad(20)$$

where H is in Oe, using for T_{1e}^{-1} the estimated direct process and the measured Raman and Orbach processes in YbES, Table II; $r_1=3.2$ Å; and $r_2=19$ Å.

A series of measurements of T_{1n}^{-1} in the supposedly identical crystals No. 6 and No. 7, Table I, was made by two methods: polarization by rotation, and then observation of the NMR signal decay at fixed θ; or saturation of the NMR signal with high rf power, and then observation of signal recovery. A plot of log signal versus time yielded a straight line whose slope determined T_{1n}^{-1}. Figure 10 shows T_{1n}^{-1} versus T for crystal No. 7 for $H=10$ kOe, $\theta=5°$, 30°, 60°, 80°, and 90°. Figure 11 shows T_{1n}^{-1} versus H at $T=1.4$°K, over the wide range $0.05\leqq H\leqq20$ kOe. The solid line in both figures is the expression

$$T_{1n}^{-1}=5.7\times10^{2}H^{-2}[3.2\times10^{-17}H^{5}\sin^{2}\theta\cos^{3}\theta\coth\chi+7\times10^{11}\exp(-60/T)+8\times10^{-2}T^{9}]\times\operatorname{sech}^{2}\chi\ \sec^{-1}.\quad(21)$$

Figure 12 shows T_{1n}^{-1} versus θ for crystal No. 6 at 10 kOe and 1.46°K; the solid line is a smooth curve through the data points, and the dashed line is

$$(T_{1n}^{-1})_{6}=2.3\times10^{-2}\sin^{2}\theta\cos^{3}\theta\coth\chi\operatorname{sech}^{2}\chi\ \sec^{-1}.\quad(22)$$

Having presented the raw data we now interpret it and explain how we arrived at Eqs. (21) and (22). Note that, except for $\theta=90°$, the form of the temperature dependence is in good agreement with expectations: $T_{1n}^{-1}\propto\exp(-60/T)$ for $T>3$°K where the Orbach process dominates (see Fig. 7), and $T_{1n}^{-1}\propto T$ for $T\leqq1.5$°K where the direct process dominates. At low temperatures and $H<1$ kOe we expect the Raman process to dominate, giving $T_{1n}^{-1}\propto H^{-2}$; for $H>5$ kOe, the direct process dominates, leading to $T_{1n}^{-1}\propto H^{2}$, approximately; both these expectations are displayed by the data in Fig. 11. At low temperature where the direct process dominates, the data of Fig. 12 show the expected θ dependence of $T_{1d}^{-1}(\theta)$ within the brackets of Eq. (20). Figure 12 does show some deviation from Eq. (22) for $0<\theta<10°$ and $80<\theta<89°$ which may be due to a residual anisotropy in Eq. (18) due to the local anisotropic distribution of the protons.

We also expect a θ-dependent contribution near $\theta=0$ from Eqs. (11). Of course the sharp peak at $\theta=90\pm1°$ is due to cross relaxation and will be discussed later.

The coefficients in Eq. (21) were determined as follows: At $T>3°$K and 10 kOe we assume the Orbach process dominates and this determines the leading factor 5.7×10^{2}; the direct process coefficient 3.2×10^{-17} then comes from fitting the data at 10 kOe, 1.45°K and $\theta=30°$, 60°; the Raman coefficient 8×10^{-2} is required to fit the low field data in Fig. (11). We note that T_{1n}^{-1} in crystal No. 6 was 1.25× that in No. 7. We often found such a variation between crystals even grown from the same solution, probably due to a variation of Yb^{3+} concentration. Over-all comparison of Eq. (21) Eq. (20) shows no serious discrepancies, considering the many approximations in the theory and the fact that Eq. (21) refers to Yb:YES and Eq. (20) refers to YbES. The fitted direct process is 4.3× smaller than the theoretical estimate and the Raman process is 5.3× larger than that measured in YbES. To summarize, proton relaxation in 2% Yb:YES is best fitted assuming

$$T_{1e}^{-1}=3.2\times10^{-17}H^{5}\sin^{2}\theta\cos^{3}\theta\coth\chi+7\times10^{-11}\times\exp(-60/T)+8\times10^{-2}T^{9}\ \text{sec}^{-1},\quad(23)$$

which we call the "revised" Yb:YES relaxation rate, and use in Sec. V in analysis of the spin refrigerator.

We now focus on the region $\theta\approx90°$ where T_{1n}^{-1} in Eq. (20) becomes very small, and the relaxation model becomes that of Sec. IVB. The data are Fig. 10(e) and the spike in Fig. 12. Actually at $\theta=90\pm1°$ the decay of the proton NMR signal was characterized not by a single exponential by an "initial" and a "final" decay rate differing by a factor ~2, but with the same

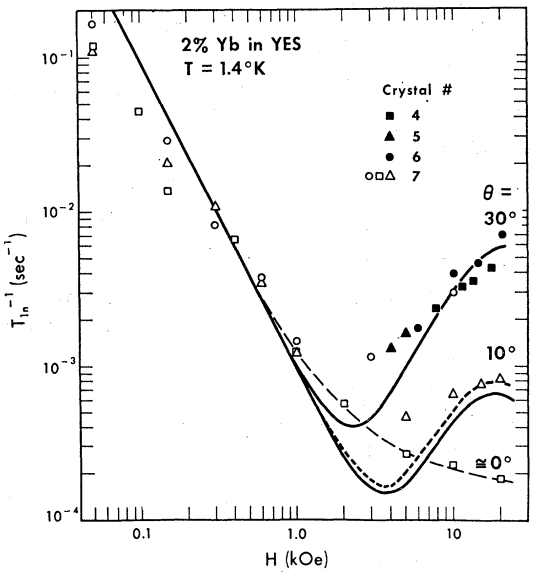

FIG. 11. Measured proton relaxation rate T_{1n}^{-1} versus H in 2% Yb:YES. The solid lines are Eq. (21).

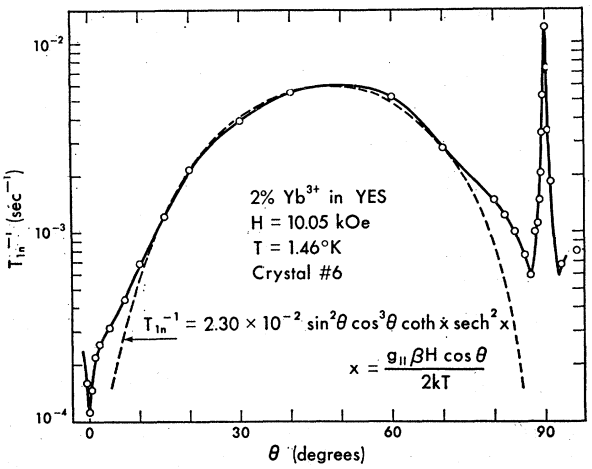

FIG. 12. Measured proton relaxation rate T_{1n}^{-1} versus θ in 2% Yb:YES. The solid line is a smooth curve through the data points.

dependence on T and θ. At $\theta=90°$, we expect from Eq. (19) $T_{12}\ll T_{1e}$, $\tau_f^{-1}\approx T_{12}^{-1}$ and $\tau_s^{-1}\approx T_{1e}^{-1}N_e/N_n$. At a small angle away from 90° such that $T_{12}\gg T_{1e}$, we expect $\tau_f^{-1}\approx T_{1e}^{-1}$, $\tau_s^{-1}=T_{12}^{-1}(\theta)N_e/N_n$. In either case the initial rate is much too slow to be associated with τ_f^{-1}, and we associate both observed rates with τ_s^{-1}. We have no ready explanation for the two slightly different rates, but note that there are two proton groups, H_2O and C_2H_5. At $\theta=90°$ and $T=1.5°$K the dominant Yb rate $T_{1R}^{-1}=8\times10^{-2}T^{9}$ with $N_e/N_n=6.06\times10^{-4}$ leads to $\tau_s^{-1}=1.8\times10^{-3}$ sec^{-1}, which is reasonably close to the rates 2.2×10^{-3} and 5.5×10^{-3} sec^{-1} in Fig. 10(e) at the same temperature. However the prediction $\tau_s^{-1}\propto T^{9}$ is not observed, but rather $\tau_s^{-1}\propto T^{4.5}$. Possibly Dy^{3+} as an impurity is contributing to the cross relaxation here, although this does not explain the temperature dependence.

In Fig. 12 the relaxation rate is reduced to half its peak value at the angle $\varphi\equiv|90-\theta|=0.3°$. This angular width of the cross relaxation peak could be due to variation of the c axis throughout the crystal or to overlap of the protons with the tail of the Yb^{3+} resonance line. At $\varphi=0.05°$ we expect $\Delta_e=\Delta_n$ and $T_{12}^{-1}\approx10^{5}$ sec$^{-1}\approx$inverse proton linewidth. At greater angles an order-of-magnitude estimate is[46]

$$T_{12}^{-1}(\varphi)\approx10^{5}\exp[-(\nu_e-\nu_n)^{2}/2\Delta\nu_e^{2}].\quad(24)$$

From Eq. (19a), the data of Fig. 12 imply $T_{12}^{-1}(\varphi=0.3°)\approx T_{1R}^{-1}\approx3$ sec^{-1} leading to a Yb^{3+} linewidth $\Delta\nu_e\approx45$ Mc/sec; this is really only an indirect order of magnitude estimate. Recent theory[47] indicates that cross relaxation falls off less rapidly than Eq. (24), so that $\Delta\nu_e$ may actually be smaller than this estimate.

[46] P. S. Pershan, Phys. Rev. **117**, 109 (1960).

[47] W. J. C. Grant, Phys. Rev. **134**, A1554 (1964); **134**, A1565 (1964); **134**, A1574 (1964); **135**, A1265 (1964).

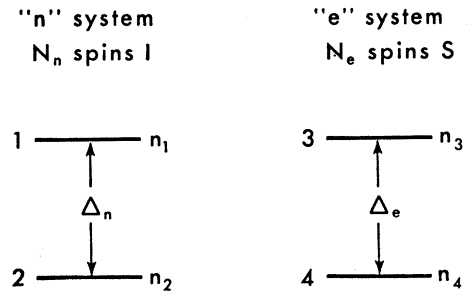

FIG. 13. Energy levels and populations for I and S spin systems.

V. ANALYSIS OF SPIN REFRIGERATOR

Sections III and IV are summarized as follows: at some given values of H, T, $\theta \neq 90°$, the Yb spin polarization p_e and the proton polarization p_n obey the simple relaxation equations

$$dp_e/dt = -(p_e - p_{e0})/T_{1e}, \tag{25a}$$

$$dp_n/dt = -(p_n - p_{n0})/T_{1n}, \tag{25b}$$

where the Yb spin-lattice relaxation T_{1e}^{-1} can be understood in terms of spin-orbit–crystal-field interactions, and the proton relaxation T_{1n}^{-1} in terms of dipolar coupling to the Yb spins. In this section we set up and solve the coupled rate equations for an I, S system *including* the cross relaxation region. Most of the results will be generally applicable to a wide variety of spin refrigerators, including the simple rotation type as well as those involving pulsed magnetic fields, combinations of ac and dc fields, and other configurations. Although the electron-spin system can represent generally any paramagnetic species with effective spin $S=\frac{1}{2}$ in dipolar coupling with any nuclear spin system $I=\frac{1}{2}$, to fix ideas, we usually refer to them as the Yb spins and the protons, respectively.

A. General Rate Equations

Consider an array of protons with Zeeman splitting Δ_n, loosely coupled to an array of Yb spins with Zeeman splitting Δ_e, as shown in Fig. 13. The populations of the levels are shown, where $n_2-n_1=n_n$, $n_2+n_1=N_n$, $n_4-n_3=n_e$, $n_4+n_3=N_e$. The Hamiltonian for the entire interpenetrating I, S, system is

$$\mathcal{H} = -\sum_i^{N_n} g_n\beta H I_{iz} + \sum_j^{N_e} \beta \mathbf{H}\cdot\mathbf{g}\cdot\mathbf{S}_j - \sum_{i,j} \frac{g_n\beta^2}{r_{ij}^3} \times \left[\mathbf{I}_i\cdot\mathbf{g}\cdot\mathbf{S}_j - \frac{3(\mathbf{r}_{ij}\cdot\mathbf{I}_i)(\mathbf{r}_{ij}\cdot\mathbf{g}\cdot\mathbf{S}_j)}{r_{ij}^2}\right], \tag{26}$$

plus similar terms for the I, I and S, S dipole-dipole interactions. The first two terms give the splittings Δ_n and Δ_e. The many terms in the dipole-dipole interaction have various effects. Terms in $I_{iz}I_{i'z}$, $S_{jz}S_{j'z}$, and $I_{iz}S_{jz}$ shift energies of individual spins and give finite linewidths to the Yb and proton resonances. Operators $I_{i+}I_{i'-}$ and $S_{j+}S_{j'-}$ induce mutual spin flips within the proton and Yb systems, respectively, and establish internal equilibrium at the transverse relaxation rates T_{2n}^{-1} and T_{2e}^{-1}. Operators $I_{i\pm}S_{jz}$ admix the zero order spin states $|M_S, m_I\rangle$; this gives rise to proton relaxation T_{1n}^{-1} through the Yb spin-lattice relaxation operator $S_+'(t)$. Finally, if $\Delta_e \approx \Delta_n$, the terms $I_{i\pm}S_{j\mp}$ induce energy conserving mutual proton-Yb spin flips at the rate w_{ij}; it is on this 1:1 cross relaxation process that we now focus attention. Of course 2:1 flips are induced if $2\Delta_n \approx \Delta_e$, etc., but we neglect multiple spin flips for the present.

Standard papers[12,15,46,47] have given the cross relaxation rate equation

$$dn_n/dt = W_{cr}(N_n n_e - N_e n_n) = -dn_e/dt, \tag{27}$$

$$W_{cr} = N_n^{-1}N_e^{-1}\sum_i^{N_n}\sum_j^{N_e} w_{ij}. \tag{28}$$

If we introduce the polarizations $p_n=n_n/N_n$, $p_e=n_e/N_e$, and define

$$\gamma \equiv N_e/(N_e+N_n), \tag{29}$$

$$T_{12}^{-1} = W_{cr}(N_e+N_n), \tag{30}$$

and include the lattice relaxation terms (25a,b), the over-all polarization-rate equations become

$$dp_n/dt = (\gamma/T_{12})(p_e-p_n) - (p_n-p_{n0})/T_{1n}, \tag{31a}$$

$$dp_e/dt = [(1-\gamma)/T_{12}](p_n-p_e) - (p_e-p_{e0})/T_{1e}. \tag{31b}$$

These equations are the basis of our analysis of the spin refrigerator, and are of course only approximations, valid if internal equilibrium is maintained in the proton and Yb spin systems, respectively, and if changes in $\mathcal{H}$ are adiabatic; i.e., occur slowly compared to the Larmor periods. These condition are met in most of our experiments, but it should be kept in mind that a more rigorous analysis involving density-matrix methods and sudden perturbation may be necessary to explain effects in spin refrigerators operating at high speed. These coupled equations can be solved exactly[48]; however $\gamma \ll 1$, and the additional well-justified approximations $T_{1n}^{-1} < T_{1e}^{-1} \ll T_{12}^{-1}$ in the cross-relation region ($\theta = 90°$) lead to

$$p_n(t) \approx [\bar{p}_n - \gamma(\bar{p}_n-\bar{p}_e) - p_{n0}]\exp(-t/\tau_s) + \gamma(\bar{p}_n-\bar{p}_e)\exp(-t/\tau_f) + p_{n0}, \tag{32a}$$

$$p_e(t) \approx [\bar{p}_n - \gamma(\bar{p}_n-\bar{p}_e) - p_{e0}]\exp(-t/\tau_s) - (1-\gamma)(\bar{p}_n-\bar{p}_e)\exp(-t/\tau_f) + p_{e0}, \tag{32b}$$

where $\bar{p}_n$ and $\bar{p}_e$ are initial values at $t=0$, and the time constants are

$$\frac{1}{\tau_s} \approx \frac{1}{T_{1n}} + \frac{(\gamma/T_{12})(1/T_{1e}-1/T_{1n})}{(1/T_{12})+(1/T_{1e})-(1/T_{1n})} \approx \frac{1}{T_{1n}} + \frac{\gamma}{T_{1e}+T_{12}}, \tag{33a}$$

$$1/\tau_f \approx 1/T_{12} + 1/T_{1e} \approx 1/T_{12}. \tag{33b}$$

[48] K. H. Langley, thesis, University of California, Berkeley, California, 1966 (unpublished).

Suppose that initially $\bar{p}_e \gg \bar{p}_n$, for example. Equation (32) shows that p_e drops in time τ_f nearly to p_n, while p_n increases by the small amount $\gamma(\bar{p}_e - \bar{p}_n)$; then $p_e \approx p_n$ and both decay together to $p_{e0} = p_{n0}$ with the long time constant τ_s. These results may be quite generally used to describe the behavior of one spin system in cross relaxation to a second, more dilute, but fast-relaxing spin system; some examples have been observed.[15,23]

B. Steady-State Proton Polarization and Buildup

In the crudest approximation we can estimate the steady proton polarization reached after many refrigerator cycles at fast rotation speeds by assuming that p_e and p_n do not vary much during a cycle, and replacing the terms in Eq. (31) by their average values over a cycle. This yields

$$\langle p_n \rangle \approx \frac{\langle p_{e0} \rangle}{1+(N_n/N_e)[\langle T_{1n}^{-1} \rangle / \langle T_{1e}^{-1} \rangle + \langle T_{1n}^{-1} / \langle T_{12}^{-1} \rangle]},$$

but a better approximation, useful at all rotation speeds, is essential for comparison to the data. The approximation we use is to break a given cycle into two regions, as indicated in Fig. 14. In region I during time τ_1, p_e, and p_n are not coupled by cross relaxation. From Eq. (25b) starting at p_{ni}, p_n reaches this value at the beginning of the cross relaxation, region II:

$$\bar{p}_n = (p_{ni} - p_{n0}) \exp(-\tau_1 R_n) + p_{n0}, \tag{34a}$$

$$R_n \equiv \langle T_{1n}^{-1} \rangle_{\tau_1}. \tag{34b}$$

In the simple rotation regrigerator R_n is obtained by averaging Fig. 12 over $-89° < \theta < 89°$, approximately. In region I, p_e obeys the more complicated equation

$$\dot{p}_e = -[p_e(t) - p_{e0}(t)]/T_{1e}(t), \tag{35}$$

where we emphasize that p_{e0} and T_{1e} both depend on $\theta(t)$. The solution of Eq. (35) is discussed in Sec. VD; for the present we merely assume that p_e starts at p_{ei} and builds up by lattice relaxation to some value $\bar{p}_e$. In region II, p_e and p_n obey Eq. (31) with initial values $\bar{p}_e$, $\bar{p}_n$ and final values p_{ef}, p_{nf}, the latter being given by Eq. (32a) with $t = \tau_2$. After many cycles a steady state is reached in which $\bar{p}_e$ and $\bar{p}_n$ no longer vary from cycle to cycle, but attain constant values, denoted by $\tilde{p}_e$ and p_{ss}, respectively, which are determined only by the operating conditions, i.e., H, T, $T_{1e}(\theta)$, $\theta(t)$, etc. In steady state $p_{ni} = p_{nf}$, $p_{ei} = p_{ef}$, $\bar{p}_n \to p_{ss}$, $\bar{p}_e \to \tilde{p}_e$. In a good refrigerator we assume operating conditions such that $\tau_1 \ll R_n^{-1}$ and $\tau_2 \ll \tau_s$ in order to prevent appreciable decay of p_n by lattice relaxation. With these approximations we find

$$p_{ss} = \frac{(\tau_1 R_n + \tau_2/\tau_s) p_{n0} + \gamma f \tilde{p}_e}{(\tau_1 R_n + \tau_2/\tau_s) + \gamma f}, \tag{36}$$

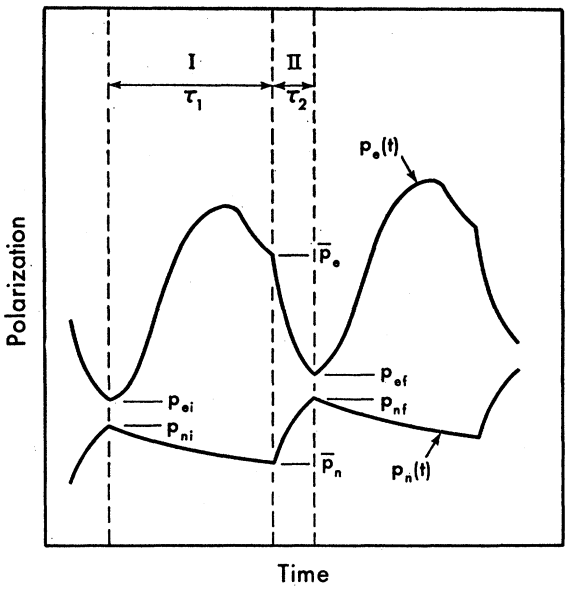

FIG. 14. Schematic illustration of Yb spin polarization p_e and proton polarization p_n in regions I and II of a spin refrigerator.

where the parameter

$$f \equiv 1 - \exp(-\tau_2/\tau_f), \tag{37}$$

is a measure of completeness of cross relaxation. For fast rotation τ_1 and $\tau_2 \to 0$, and Eq. (36) predicts that the proton polarization approaches $\tilde{p}_e$, the Yb spin polarization in the cross relaxation region.

To examine the dynamics of buildup of p_n we first make a simple calculation assuming that $\bar{p}_e$ very quickly reaches $\tilde{p}_e$, i.e., $\tau_1^{-1} \ll \langle T_{1e}^{-1} \rangle_{\tau_1}$, and then make corrections in Sec. VC. The change in p_n per cycle is $(\Delta p_n/\Delta n) = p_{nf} - p_{ni}$, where $n = t/(\tau_1 + \tau_2)$ is the number of cycles. Assuming $\tau_2 \ll \tau_s$, $\tau_1 \ll R_n^{-1}$ as before, we obtain an effective rate equation which shows that $p_n \to p_{ss}$ exponentially at a rate

$$1/\tau_{0n} \approx (1/\tau_1)[\tau_1 R_n + \tau_2/\tau_s + \gamma f]. \tag{38}$$

In Eq. (36) and Eq. (38) it is well justified in our rotation regrigerator to neglect τ_2/τ_s compared to $\tau_1 R_n$, and we do so in the following.

C. Corrections

Multiple spin flips. It is energetically favorable for m Yb spins to flip n protons if $m\Delta_e = n\Delta_n$. If we assume that all cross relaxation occurs when Δ_e and Δ_n are commensurable, but not necessarily 1:1, and that energy is exactly conserved, then Eq. (36) and Eq. (38) are modified to become Eqs. (40a) and (40b) below, where

$$\epsilon \equiv \Delta_e/\Delta_n. \tag{39}$$

These equations also include other corrections but if $K \to 1$, Eq. (40a) shows that multiple spin flips can

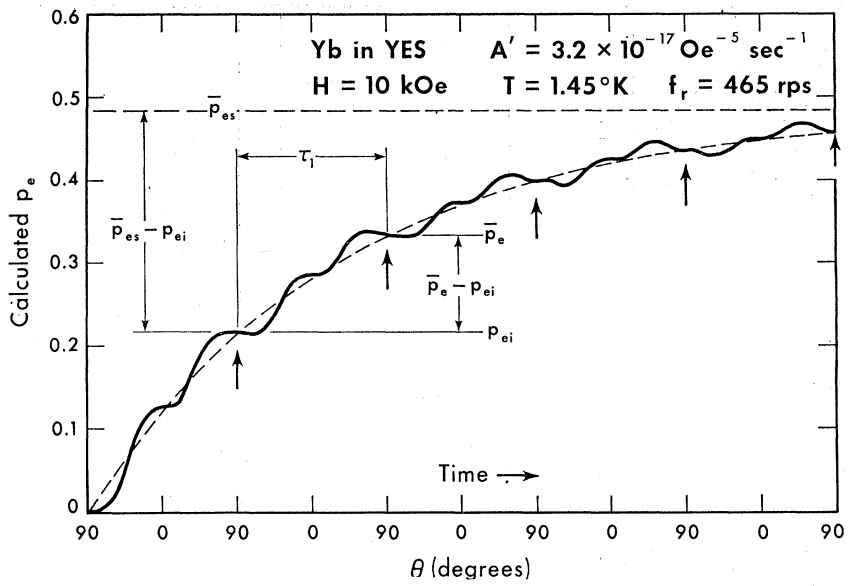

FIG. 15. Calculated $p_e(\theta)$ versus θ for Yb:YES.

reduce the limiting value of the proton polarization by the factor ϵ.

Incomplete Yb *spin polarization.* Equations (36) and (38) are based on the assumption that $\bar{p}_e \approx \tilde{p}_e$ throughout the buildup of p_n, but if the buildup of $\bar{p}_e$ is also taken into account one finds[48]

$$p_{ss}=\frac{\tau_1 R_n p_{n0}+[\epsilon\gamma f K\bar{p}_{es}/(K+f(1-K))]}{\tau_1 R_n+[\epsilon^2\gamma f K/(K+f(1-K))]}, \quad (40a)$$

$$\frac{1}{\tau_{0n}}=\frac{1}{\tau_1}\left\{\tau_1 R_n+\frac{\epsilon^2\gamma f[K/(1-K)-\tau_1 R_n]}{K/(1-K)-\tau_1 R_n+f}\right\}, \quad (40b)$$

where $\bar{p}_{es}$ is the steady state value of p_e at $\theta=90°$ found by solving Eq. (35), nelgecting the effect of the protons on the Yb polarization. The parameter K, defined by

$$K\equiv 1-\exp(-\tau_1 R_e), \quad R_e\equiv\langle T_{1e}^{-1}\rangle_{\tau_1}, \quad (41)$$

is a measure of the completeness of lattice relaxation of p_e in region I. If $K\rightarrow 1$, assumed in Sec. VB, then $\tilde{p}_e\rightarrow\bar{p}_{es}$.

D. Yb Spin Polarization

Since p_{ss} depends on $\bar{p}_{es}$ (and in fact, $p_{ss}\rightarrow\bar{p}_{es}$, ideally) we must solve for the dynamic behavior of p_e. For simple rotation $\theta=\omega_r t=2\pi f_r t$, and Eq. (35) becomes

$$\frac{dp_e(\theta)}{d\theta}=-\frac{p_e(\theta)-p_{e0}(\theta)}{\omega_r}T_{1e}^{-1}(\theta), \quad (42)$$

which can be written in the general form, also suitable for other refrigerators,

$$dp_e/d\theta+P(\theta)p_e=Q(\theta), \quad (43)$$

where P and Q are periodic with period π. The general solution of Eq. (43) is[49]

$$p_e(\theta)=\exp\left[-\int_{\theta_0}^{\theta}P(\theta')d\theta'\right]\times\left\{\int_{\theta_0}^{\theta}\exp\left[\int_{\theta_0}^{\theta}P(\theta'')d\theta''\right]Q(\theta')d\theta'+p_e(\theta_0)\right\}. \quad (44)$$

Using Eq. (44) we can write an expression for $p_e(\theta+\pi)$, which after initial transients must equal $p_e(\theta)$ in the

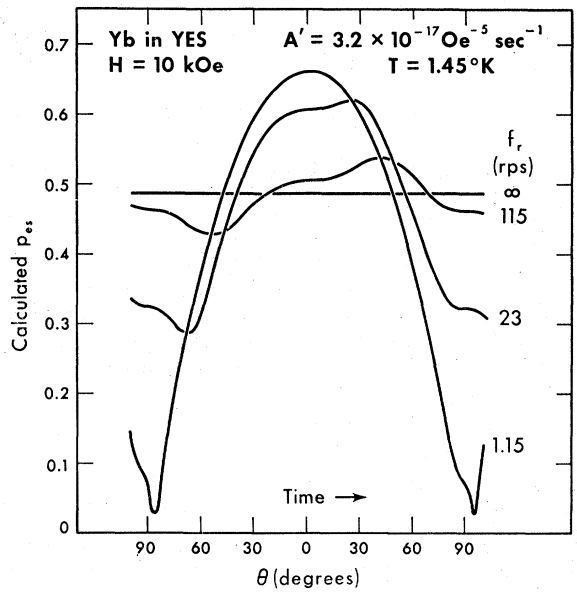

FIG. 16. Calculated $p_{es}(\theta)$ versus θ for Yb:YES at various rotation frequencies f_r.

[49] See, e.g., H. B. Dwight, *Tables of Integrals and Other Mathematical Data*, 4th ed. (The Macmillan Company, New York, 1964).

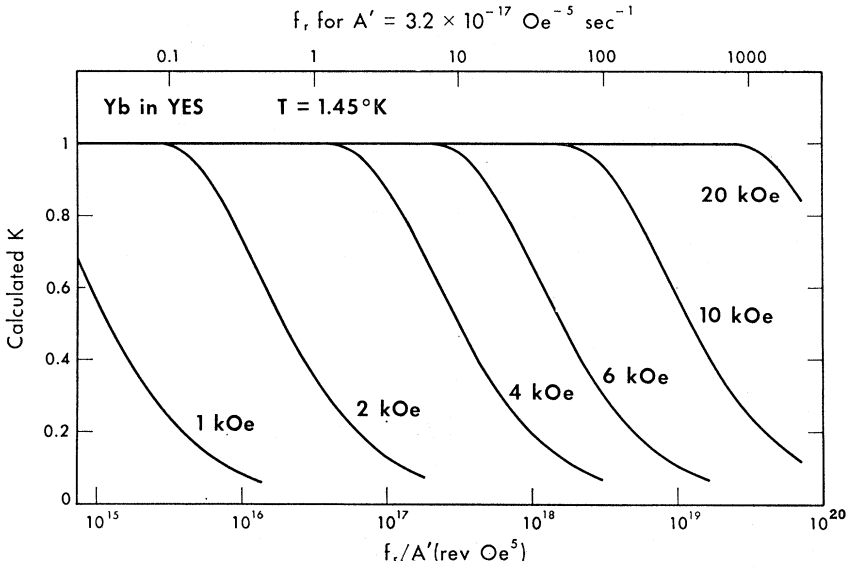

FIG. 17. Calculated value of the parameter K, Eq. (46), for Yb:YES.

steady state, defined by $p_{es}(\theta)$, and given by

$$p_{es}(\theta)=\frac{1-K}{K}\int_{\theta}^{\theta+\pi}\exp\left[\int_{\theta}^{\theta'}P(\theta'')d\theta''\right]Q(\theta')d\theta', \quad (45)$$

$$K\equiv 1-\exp\left[-\int_{0}^{\pi}P(\theta)d\theta\right]. \quad (46)$$

Equation (46) is equivalent to the earlier definition Eq. (41). Equations (45) and (46) may be used to express the integrals in $p_e(\theta+\pi)$ and to show

$$p_e(\theta+\pi)-p_e(\theta)=K[p_{es}(\theta)-p_e(\theta)], \quad (47a)$$

valid for any θ; taking $\theta=\pi/2$ and defining $p_{es}(\pi/2)=\bar{p}_{es}$ we obtain

$$\bar{p}_e-p_{ei}=K(\bar{p}_{es}-p_{ei}), \quad (47b)$$

which states that the increase in p_e in any cycle is just the fraction K of the increase after many cycles. If $K\ll 1$, $\bar{p}_e$ builds up to $\bar{p}_{es}$ after n cycles according to

$$\bar{p}_e=\bar{p}_{es}[1-\exp(-Kn)]. \quad (48)$$

In the limit $f_r\to\infty$ it follows from Eq. (45) that $p_{es}(\theta)$ becomes independent of θ and is equal to

$$(p_{es}(\theta))_\infty=(\bar{p}_{es})_\infty$$

$$=\int_0^{\pi}p_{e0}(\theta)T_{1e}^{-1}(\theta)d\theta\Big/\int_0^{\pi}T_{1e}^{-1}(\theta)d\theta. \quad (49a)$$

As $f_r\to 0$, $p_{es}(\theta)\to p_{e0}(\theta)$. For Yb:YES Eq. (49a) becomes

$$(\bar{p}_{es})_\infty=(32/15\pi)g_{11}\beta H/2kT. \quad (49b)$$

If T_{1e}^{-1} were assumed isotropic, Eq. (49a) yields the slightly smaller value $(\bar{p}_{es})_\infty=(2/\pi)[g_{11}\beta H/2kT]$, showing that electron spins with isotropic relaxation can still be used as nuclear spin refrigerators provided that $f_r\gg T_{1e}^{-1}$ and that the g factor is sufficiently anisotropic. In practice however the larger anisotropy in T_{1e}^{-1} for Yb:YES is a significant advantage, permitting lower operating frequencies.

E. Numerical Calculations for Rotation of Yb:YES

We have calculated with an IBM 1620 computer numerical solutions for $p_e(\theta)$ in Yb:YES by two methods. The first integrates in Eq. (44) to find the instantaneous value $p_e(\theta)$ showing dynamic approach to steady state, Fig. 15; integrates in Eq. (45) to show the periodic behavior of $p_{es}(\theta)$, Fig. 16; and integrates in Eq. (46) to find K, Fig. 17. The second method directly integrates Eq. (42) by the method of Runge and Kutta.[50] We have assumed throughout $p_{e0}(\theta)=\tanh(g_{11}\beta H\cos\theta/2kT)$, $g_{11}=3.43$, $T=1.45°$K, $T_{1e}^{-1}(\theta)=4T_{1e}^{-1}(45°)\sin^2\theta\cos^2\theta$, $T_{1e}^{-1}(45°)=A'\sin^2 45°\cos^3 45°\times H^5\coth(g_{11}\beta H\cos 45°/2kT)$, and $A'=3.2\times 10^{-17}$ from Eq. (23).

Figure 15 shows the growth of p_e from zero at $f_r=465$ rps, $H=10$ kOe; the dashed line is from Eq. (48) using K from Fig. 17. The arrows indicate the points at which cross relaxation to the protons occurs. Figure 16 shows the steady state $p_{es}(\theta)$ over one cycle: as $f_r\to 0$, $p_{es}(\theta)$ follows $p_{e0}(\theta)$ except for some lag at 0° and 90° where T_{1e} is very long. As $f_r\to\infty$, $p_{es}(\theta)$ becomes constant and is given by Eq. (49a). Figure 18 shows that $\bar{p}_{es}$ becomes constant above a certain frequency of order $10^{-1}\langle T_{1e}^{-1}\rangle$, which depends on H. This frequency saturation is also evident in Fig. 19, which is a cross plot of $\bar{p}_{es}$ versus H. For a given f_r, $\bar{p}_{es}\propto H$ up to a certain value, and then decreases like $\bar{p}_{es}\propto H^{-1/3}$, as it turns out, because T_{1e}

[50] See, e.g., F. B. Hildebrand, *Introduction to Numerical Analysis* (McGraw-Hill Book Company, Inc., New York, 1956).

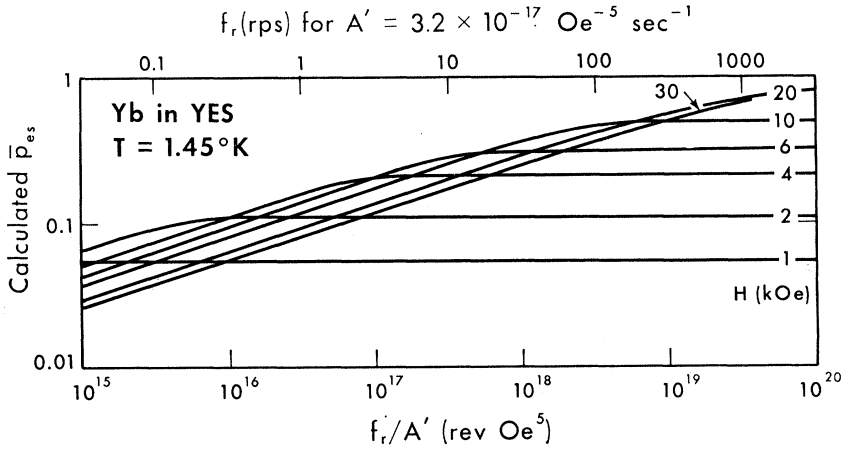

FIG. 18. Calculated value of $\bar{p}_{es}$ versus f_r for Yb:YES.

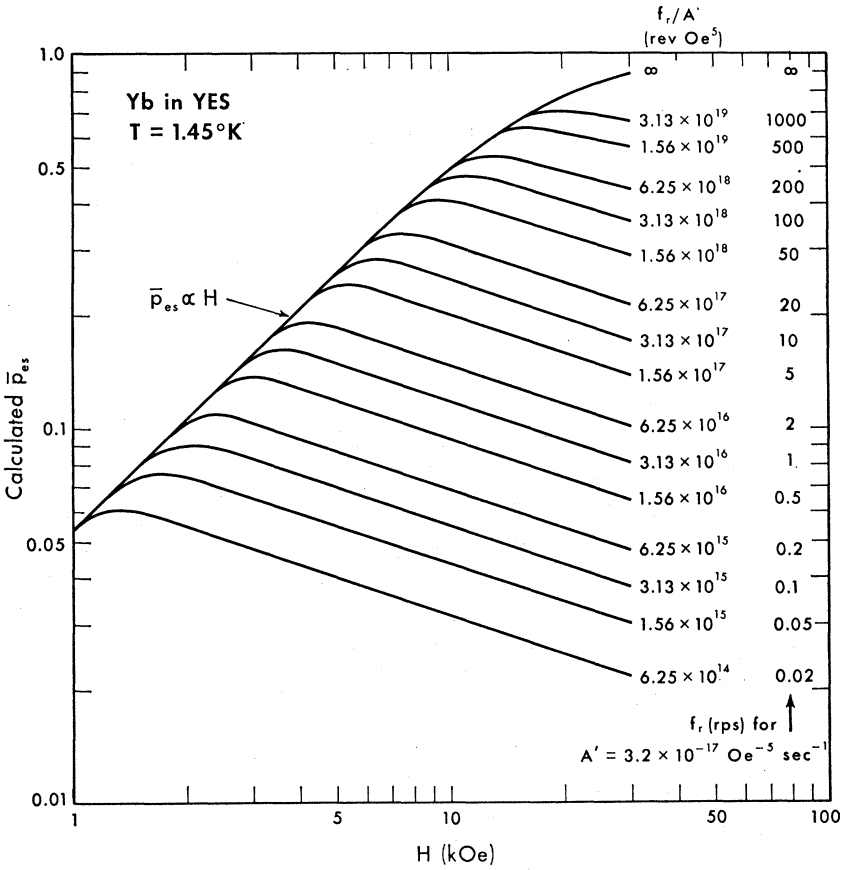

FIG. 19. Calculated value of $\bar{p}_{es}$ versus H for Yb:YES.

is becoming so short compared to f_r^{-1} that p_e follows p_{e0} as $\theta \rightarrow 90°$. Similarly for frequencies below saturation $\bar{p}_{es} \propto f^{1/3}$ in Fig. 18. Since A' is not known precisely but appears in Eq. (42) in the form $\omega_r T_{1e} \propto f_r/A'$, we indicate this parameter in Figs. 18 and 19 so that they can be used for other values of A' should better data become available.

Rotation of an anisotropic crystal in a magnetic field produces heating through non resonant paramagnetic relaxation losses, analogous to the loss due to the complex susceptibility in an oscillating field.

An estimated upper limit is

$$Q \approx \frac{N_e(g\beta H_0)^2}{8kTT_{1e}} \times \frac{(\omega T_{1e})^2}{1+(\omega T_{1e})^2} \text{ ergs cm}^{-3} \text{ sec}^{-1}.$$

For typical values $N_e \sim 10^{19}$, $g \sim 2$, $T \sim 1°$K, $(\omega T_{1e})^2 \sim 1$, $H \sim 10^4$ Oe, $T_{15} \sim 10^{-3}$ sec we find $Q \sim 10^{-1}$ W per cm³ of

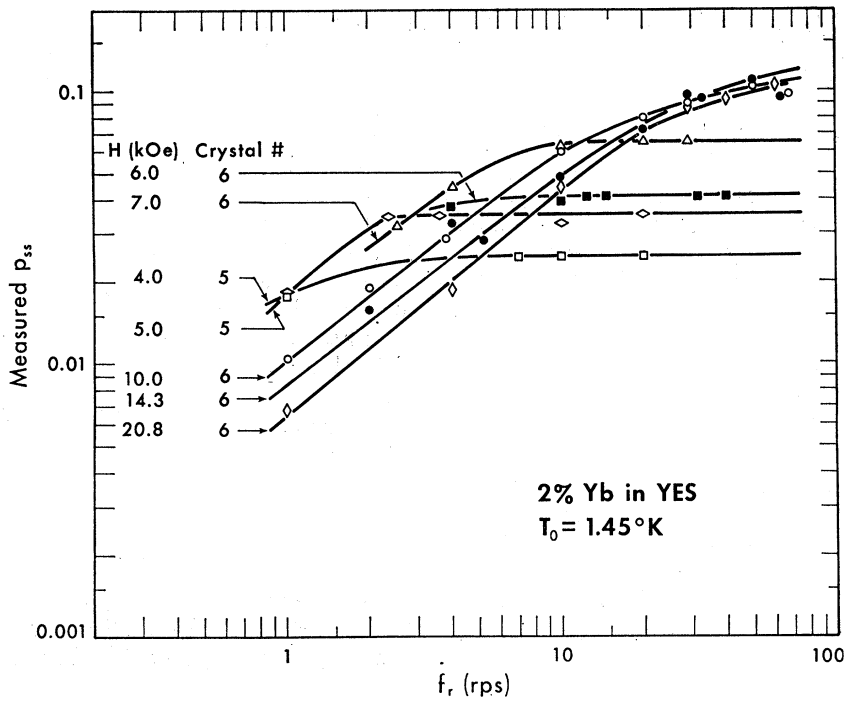

FIG. 20. Measured steady-state proton polarization p_{ss} versus rotation frequency f_r for Yb:YES.

crystal. Actually the calculation for a rotating field, anisotropic g, and anisotropic T_{1e} is considerably more complicated, requiring a computor calculation, but the magnitude of Q will be the same. A good crystal cooled by immersion in superfluid He^4 will probably not rise more than 20% above bath temperature with such a heat input. We have not detected this relaxation heating because it has been dominated by bearing friction in the present apparatus, but it is not a negligible effect. Since the proton polarization time is $\sim 10^{-2}$ of the relaxation time, there need be no large helium losses over extended periods as in the microwave method.

Although we have implicitly assumed that the crystal c axis is in the horizontal plane, as in Fig. 1, this is not strictly required for a Yb:YES spin refrigerator, since if c is at some angle $\Theta < 90°$ with the vertical, this only reduces the maximum g factor to $g_{11}\sin\Theta$ but still allows $\theta = 90°$ at some time during the cycle since $g_\perp = 0$ in the whole plane perpendicular to c. For a single crystal the ideal proton polarization will be reduced by $\sin\Theta$, and for a random powdered sample by $\pi/4$. This is of considerable practical significance, and suggests the possibility of polarization of the protons in a highly hydrogeneous medium in which crystallites of Yb:YES are dispersed.

VI. PROTON POLARIZATION EXPERIMENTS IN Yb:YES

We performed polarization experiments on the crystals of Table I by mounting them in the holder of the apparatus, Fig. 4, with Kel-F grease, and measuring first the proton NMR signal proportional to $p_{n0}(H,T_0)$ in a given field H and temperature T_0. Then the crystal was rotated at some constant speed f_r, while we observed the build up rate τ_{0n}^{-1} and the final steady state enhanced proton signal $p_{\rm enh}(f_r,H,T)$. Bearing friction caused a slight temperature rise, $T \approx 1.2T_0$, typically, which depended on f_r. We define the measured enhancement $E = p_{\rm enh}(f_r,H,T)/p_{n0}(H,T_0)$ and the "measured" steady state polarization $p_{ss} = Ep_{n0}(H,T_0)$, which is essentially the proton polarization that would have obtained without heating. In this way we adjust the data of a run to a constant temperature. Experiments were made over the ranges $1.4 \leqq H \leqq 20.7$ kOe, $1.2 \leqq T \leqq 2.7$°K, $0.5 \leqq f_r \leqq 70$ rps for 0.5%, 2%, 10% Yb:YES and 2% Yb^{172}:YES. Our primary objectives were to study the dependence of p_{ss} and τ_{0n} on H, f_r, and Yb concentration, and to obtain as large a proton polarization as possible.

Before presenting the data we review the theoretical expectations: p_{ss} is given by Eq. (40a) by replacing τ_1 by $1/(2f_r)$. This complicated expression includes corrections ϵ for multiple flips, f for incomplete cross relaxation, and K for incomplete Yb polarization, but in the ideal case these parameters each approach unity, so that

$$p_{ss} \approx (R_n p_{n0} + 2\gamma f_r \bar{p}_{es})/(R_n + 2\gamma f_r), \qquad (50)$$

where typical values are $R_n = \langle T_{1n}^{-1} \rangle_\theta \approx 3\times 10^{-3}$ sec^{-1} (Fig. 12), $\gamma = (N_e/N_n) \approx 6\times 10^{-4}$ (for 2% Yb), and $\bar{p}_{es}$ is given by Figs. 18 and 19. The predicted behavior

of p_{ss} versus f_r at constant H is thus: at low f_r, both terms in the numerator and denominator of Eq. (50) are significant, and p_{ss} increases from p_{n0} as f_r increases from zero. At intermediate values of f_r, the second terms dominate and $p_{ss}\approx\bar{p}_{es}(f_r)\propto f_r^{1/3}$ up to the saturation region where $p_{ss}=\bar{p}_{es}$ becomes constant at high frequencies. Thus, except for $f_r\lesssim 5$ rps, we expect p_{ss} versus f_r and p_{ss} versus H to resemble closely the curves $\bar{p}_{es}$ versus f_r and $\bar{p}_{es}$ versus H of Figs. 18 and 19. In fact at high frequencies, Eq. (40a) becomes $p_{ss}=\bar{p}_{es}/\epsilon$ even for small values of f and K, so that only multiple flips, which may depend on f_r and H, should keep the proton polarization from reaching the ideal value $\bar{p}_{es}$, the steady state Yb polarization at $\theta=90°$.

Figure 20 shows the measured p_{ss} versus f_r for two supposedly identical 2% crystals for fields in the range 4 to 20 kOe; Fig. 21 is a cross plot of these data p_{ss} versus H. Figure 20 does indeed exhibit qualitative agreement with Fig. 18: p_{ss} saturates at successively lower f_r at lower H; and the saturated value is lower for lower H. Likewise the general resemblance of Fig. 21 to Fig. 19 is striking. Although $\bar{p}_{es}\propto H$ at low fields, Fig. 21 shows $p_{ss}\propto H^{1.6}$; we later ascribe this discrepancy to a field dependence of ϵ. The measured proton polarization reaches its peak at roughly the same field as $\bar{p}_{es}$. Actually the positions of the maxima in Fig. 21 are determined by A', taken to be 3.2×10^{-17} Oe^{-5} sec^{-1} from proton relaxation data. The value $A'=1.9\times10^{-17}$ Oe^{-5} sec^{-1} gives the best correspondence between the maxima of Figs. 19 and 21.

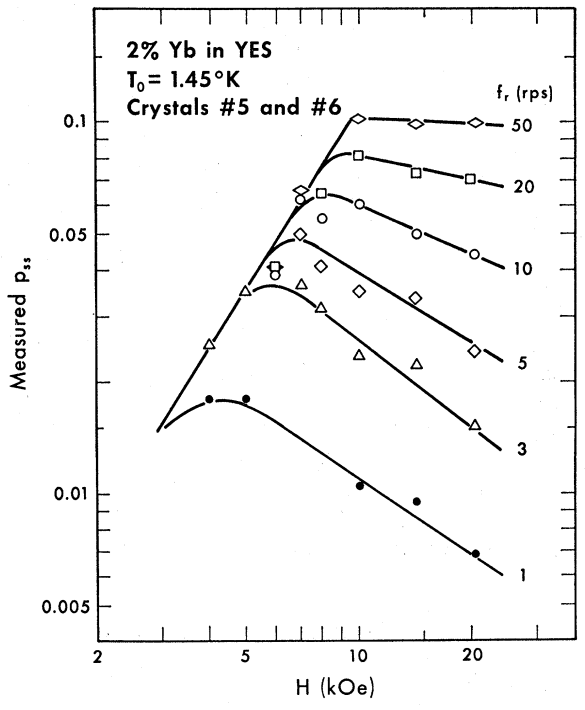

FIG. 21. Measured steady-state proton polarization p_{ss} versus field H for Yb:YES.

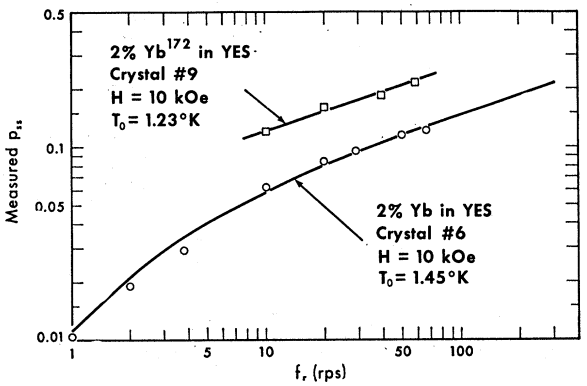

FIG. 22. Measured steady-state proton polarization p_{ss} versus f_r for two crystals.

The frequency-saturated value of p_{ss} was found to be the same for 0.5%, 2%, and 10% crystals at the same field; this is expected from Eq. (50), since γ cancels out at high frequencies.

Figure 22 shows the measured p_{ss} versus f_r for two crystals, 2% Yb:YES at $T_0=1.45°K$, and 2% Yb^{172}: YES at $T_0=1.23°K$. In the latter, at 60 rps the temperature rose to 1.42°K, and the measured enhancement was $E=259$, corresponding to an actual proton polarization of 18.6% at 1.42°K. The calculated value of $\bar{p}_{es}$ is 42% under these conditions. The data clearly show that frequency saturation was not reached and that considerably higher polarizations would be obtained at higher rotation speeds. It may be more practical to rotate the field rapidly rather than the crystal; a rotating field magnet at $f_r\sim10^3$ cps is being constructed.

Although the qualitative behavior of p_{ss} versus f_r and H is reasonably understood, more exact comparisons of Figs. 20, 21, and 22 with Figs. 18 and 19 show that the magnitude of the p_{ss} even in the saturated region is several times smaller than $\bar{p}_{es}$. As a first and probably incorrect attempt to explain this we consider A' an adjustable parameter and fit the data of Fig. 22 to the form of Eq. (50) by taking $\bar{p}_{es}=\alpha f_r^{1/3}$ and varying α and γ/R_n to give the best fit; varying α is equivalent to varying A'. The lower curve in Fig. 22 is the result with $\gamma/R_n=0.25$ sec, $\alpha=0.0316$, and $A'=1.5\times10^{-15}$ Oe^{-5} sec^{-1}; the upper curve for the enriched crystal is drawn with $A'=2.8\times10^{-16}$ Oe^{-5} sec^{-1}. These two values of A' are much larger than either the value from proton relaxation or the theoretical estimate. Furthermore, adjusting A' cannot alter the frequency saturated value of p_{ss}, but only the frequency at which it sets in. We feel that the low values of p_{ss} are best explained by multiple spin flips.

To consider this possibility we attempt to fit the p_{ss} data of Fig. 21 with Eq. (40a), with $f=1$, K from Fig. 17, $\bar{p}_{es}$ from Fig. 19, and $\epsilon=\epsilon_{\rm eff}(H,f_r)$, an adjustable parameter required to fit the data, given by

$$\epsilon_{\rm eff}\cong\tfrac{1}{2}(\bar{p}_{es}/p_{ss})+\tfrac{1}{2}[\bar{p}_{es}^2/p_{ss}^2-2R_n/\gamma f_r]^{1/2}. \quad (51)$$

Figure 23 shows the empirically determined values ϵ_{eff} versus H for various frequencies, and suggests that multiple flips are more probable at lower f_r and lower H. This is not unexpected since at low f_r more time is spent at orientations where multiple flips can occur, allowing more Yb spin polarization to leak to the protons at higher effective spin temperatures before θ reaches 90°. At lower H the fractional linewidth $\Delta H/H$ may be greater, allowing more overlap in the tails at a given θ. A quantitative theory would be complex; there is yet no good data on the Yb linewidth or even the mechanism of the linewidth.

In Eq. (40b) $\tau_1 R_n$ is dominated by $K/(1-K)$, leading to the buildup rate

$$1/\tau_{0n}=R_n+2\epsilon^2\gamma f K f_r/[K+f(1-K)]. \quad (52)$$

We expect τ_{0n}^{-1} versus f_r to start at R_n and increase linearly with f_r until the onset of frequency saturation of $\bar{p}_{es}$ (implying $K<1$), or insufficient cross relaxation (implying $f<1$), or decrease of ϵ. Any of these would cause τ_{0n}^{-1} to increase more slowly than linearly with f_r. The data are not good enough to establish this effect. If ϵ, K, and f are simply set to unity we obtain

$$\tau_{0n}^{-1}=R_n+2\gamma f_r, \quad (53)$$

which predicts for $f_r>10$ rps, $\tau_{0n}^{-1}\approx 2\gamma f_r$, which is just proportional to the Yb concentration and the rotation frequency, and independent of H and T. The buildup was observed to be exponential with a time constant ranging from 10 to 1000 sec, and very roughly given by Eq. (53), although the data have a bad scatter. Table III shows the value of R_n and γ required to fit the data, along with values from proton relaxation data and growing solution concentration. For $f_r>10$ rps, τ_{0n}^{-1} appears to be roughly independent of H and T. Unfortunately the data are not extensive enough to verify Eq. (52) or Eq. (53), and we can only say that the number of cycles for buildup is of the order of $\gamma^{-1}=N_n/N_e$, as expected from elementary considerations. We feel that the factor f, Eq. (37), must be of order unity even at $f_r\approx 60$ rps where $\tau_2\approx 10^{-4}$ sec, indicating that $\tau_f\approx T_{12}$ must be at least as short as 10^{-4} sec.

TABLE III. Average proton relaxation rate R_n; ratio of Yb ion concentration to proton concentration γ.

	R_n(sec^{-1})		γ	
	From τ_{0n} data	From proton relaxation data	From τ_{0n} data	From growing solution concentration
0.5% Yb in YES crystal No. 3	2.2×10^{-3}	1×10^{-3}	5.4×10^{-4}	1.5×10^{-4}
2% Yb in YES crystals No. 5,6,7	1.1×10^{-2}	3×10^{-3}	6.4×10^{-4}	6.06×10^{-4}
10% Yb in YES crystal No. 2	4.8×10^{-2}	2×10^{-2}	7.4×10^{-3}	3.03×10^{-3}

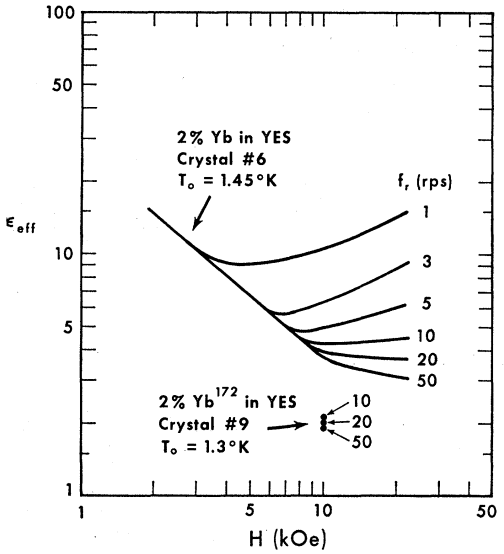

FIG. 23. Emperical factor ϵ_{eff} from Eq. (51).

VII. SUMMARY AND CONCLUSIONS

By rotating single crystals of 2% Yb:YES at 60 rps in 10 kOe at 1.42°K we have obtained up to ~19% polarization of the protons, which is about half the calculated polarization of the Yb spins at the cross relaxation region under these operating conditions. The discrepancy is probably due to insufficient rotation speed and multiple proton-Yb spin flips. The dependence of the steady-state proton polarization on frequency and field is in good qualitative agreement with a simple rate-equation theory assuming only cross relaxation and spin-lattice relaxation terms.

Proton relaxation over the range $0<\theta<89°$ agrees with a shell-of-influence model in both magnitude and dependence on H and T. These data are used to indirectly infer the direct-processes relaxation rate for Yb^{3+}, which is crucial to the interpretation of the spin refrigerator dynamics; unfortuntaely there is yet no direct measurement of this relaxation rate. Proton relaxation at $\theta=90\pm1°$ shows a sharp spike due to cross relaxation with the Yb spins. There is no experimental or theoretical evidence that g_1 for Yb:YES does not become at least as small as $g_n=0.003$ in fields up to ~20 kOe.

The proton polarization builds up as quickly as 10 sec, the magnetic field is not required to be homogeneous, and the average heat input to the helium bath can be made negligible if friction losses are eliminated, e.g., by rotating the field rather than the crystal. It is not unreasonable to expect proton polarizations of ~50% in higher fields (20 kOe) and faster rotation speeds (10^3 rps). Yb:YES is 5% hydrogen by weight, compared to 3% for $(Nd,La)_2Mg_3(NO_3)_{12}\cdot 24\,H_2O$ used in the microwave dynamic polarization method. The possible use of a Yb:YES spin refrigerator as a polarized

target is suggested, but the optimum configuration cannot yet be specified; a pulsed rotating field[17] or a combination of dc and oscillating fields may be more effective than a simple rotating field.

ACKNOWLEDGMENTS

We wish to acknowledge with much thanks the help of Dr. T. J. Schmugge in the initial stages of this work; many helpful discussions with J. R. McColl on the the theory of spin refrigerators and computer programming; the able assistance of R. L. Ballard in computing the Yb polarization; and the calculation of the Yb:YES relaxation by Dr. G. H. Larson. This research has been supported in part by the U. S. Office of Naval Research and the U. S. Atomic Energy Commission; this paper is AEC document report code No. UCB-34P20-35.

PHYSICAL REVIEW VOLUME 152, NUMBER 1 2 DECEMBER 1966

Optical Absorption of Tetrahedral Fe^{2+} ($3d^6$) in Cubic ZnS, CdTe, and $MgAl_2O_4$

G. A. SLACK, F. S. HAM, AND R. M. CHRENKO
General Electric Research and Development Center, Schenectady, New York
(Received 17 June 1966)

The optical absorption spectrum of substitutional Fe^{2+} ions at concentrations from 2×10^{18} to 4×10^{20} cm^{-3} has been studied for cubic ZnS, CdTe, and $MgAl_2O_4$ single crystals from 3 to 300°K. The Fe^{2+} ions show a single broad absorption band at 300°K in the infrared region between 1500 and 7500 cm^{-1} (1.3 to 6.7 μ) that arises from the $^5E \rightarrow {}^5T_2$ transition. At low temperatures this band shows many distinct lines which are identified as resulting from zero-phonon and phonon-assisted transitions between the spin-orbit levels of ^5E and $^5T_2$ in tetrahedral symmetry. The levels of ^5E are found to be described well by crystal-field theory: There are five uniformly spaced levels split in second order by spin-orbit interactions, with an interval given by 15, 10, and 13 cm^{-1} for Fe^{2+} in ZnS, CdTe, and $MgAl_2O_4$, respectively. The levels of $^5T_2$ do not fit the predictions of crystal-field theory; they can, however, be understood if a moderately strong Jahn-Teller effect occurs in the $^5T_2$ state, so that the first-order spin-orbit splitting of $^5T_2$ is quenched to a small fraction of its crystal-field value. Values for this Jahn-Teller energy of 535, 255, and 945 cm^{-1} are derived from the data for ZnS, CdTe, and $MgAl_2O_4$, respectively. A phenomenological Hamiltonian is found which describes the dynamical Jahn-Teller effects in ZnS very well, and which may also be appropriate for $MgAl_2O_4$ but does not suffice for CdTe. An alternative interpretation of the spectrum for Fe^{2+} in ZnS, not requiring so strong a Jahn-Teller effect, more nearly accords with the predictions of crystal-field theory, but at the expense of assuming that some of the observed zero-phonon lines arise from Fe^{2+} associated with some other defect common to all samples, or from a mixture of cubic and hexagonal regions within the crystals. Values of the cubic-field parameter Dq for Fe^{2+} in these crystals are -340, -248, and -447 cm^{-1} for ZnS, CdTe, and $MgAl_2O_4$, respectively. The phonon-assisted transitions yield values for the transverse acoustic, longitudinal acoustic, transverse optic, and longitudinal optic phonons in ZnS and CdTe which are 115, 184, 296, 331 cm^{-1} and 65, 105, 140, 180 cm^{-1}, respectively.

I. INTRODUCTION

THE optical absorption spectra of ions of the first transition series in tetrahedral coordination in various crystalline solids have been studied in a number of investigations.[1–21] These spectra are of interest for comparison with the more familiar spectra of these ions in octahedral coordination, and as a test of the applicability of crystal-field theory to the tetrahedral case. The purpose of this paper is to report observations on the optical absorption spectra of tetrahedral Fe^{2+} in cubic ZnS, CdTe, and $MgAl_2O_4$ over the tem-

[1] W. W. Coblentz, Carnegie Instit. Wash. Publ. **97**, 1908, Part VI, p. 57.
[2] D. S. McClure, J. Phys. Chem. Solids **3**, 311 (1957).
[3] W. Low and M. Weger, Phys. Rev. **118**, 1119 (1960); **118**, 1130 (1960).
[4] R. Pappalardo, D. L. Wood, and R. C. Linares, Bull. Am. Phys. Soc. **5**, 516 (1960).
[5] R. E. Dietz and R. Pappalardo, Bull. Am. Phys. Soc. **5**, 416 (1960); **6**, 110 (1961).
[6] R. Pappalardo, J. Mol. Spectr. **6**, 554 (1961).
[7] R. Pappalardo and R. E. Dietz, Phys. Rev. **123**, 1188 (1961).
[8] R. Pappalardo, D. L. Wood, and R. C. Linares, J. Chem. Phys. **35**, 1460 (1961).
[9] R. Pappalardo, D. L. Wood, and R. C. Linares, J. Chem. Phys. **35**, 2041 (1961).
[10] H. A. Weakliem and D. S. McClure, J. Appl. Phys. **33**, 347S (1962).
[11] H. A. Weakliem, J. Chem. Phys. **36**, 2117 (1962).
[12] J. Ferguson, J. Chem. Phys. **39**, 116 (1963).
[13] J. W. Allen, Physica **29**, 764 (1963).
[14] R. E. Dietz, H. Kamimura, M. D. Sturge, and A. Yariv, Phys. Rev. **132**, 1559 (1963).
[15] D. S. McClure, J. Chem. Phys. **39**, 2850 (1963).
[16] R. Pappalardo, Spectrochim. Acta **19**, 2093 (1963).
[17] A. I. Ryskin, G. I. Khil'ko, B. I. Maksakov, and K. K. Dubenskii, Opt. i Spektroskopiya **16**, 274 (1962) [English transl.: Opt. Spectr. **16**, 149 (1964)].
[18] S. Ibuki and D. Langer, J. Phys. Soc. Japan **19**, 422 (1964).
[19] G. A. Slack, Phys. Rev. **134**, A1268 (1964).
[20] D. Langer and S. Ibuki, Phys. Rev. **138**, A809 (1965).
[21] I. Broser, H. Maier, and H. J. Schulz, Phys. Rev. **140**, A2135 (1965).